iScience

CellPress
OPEN ACCESS

Article

T cells regulate lymph node-resident ILC populations in a tissue and subset-specific way

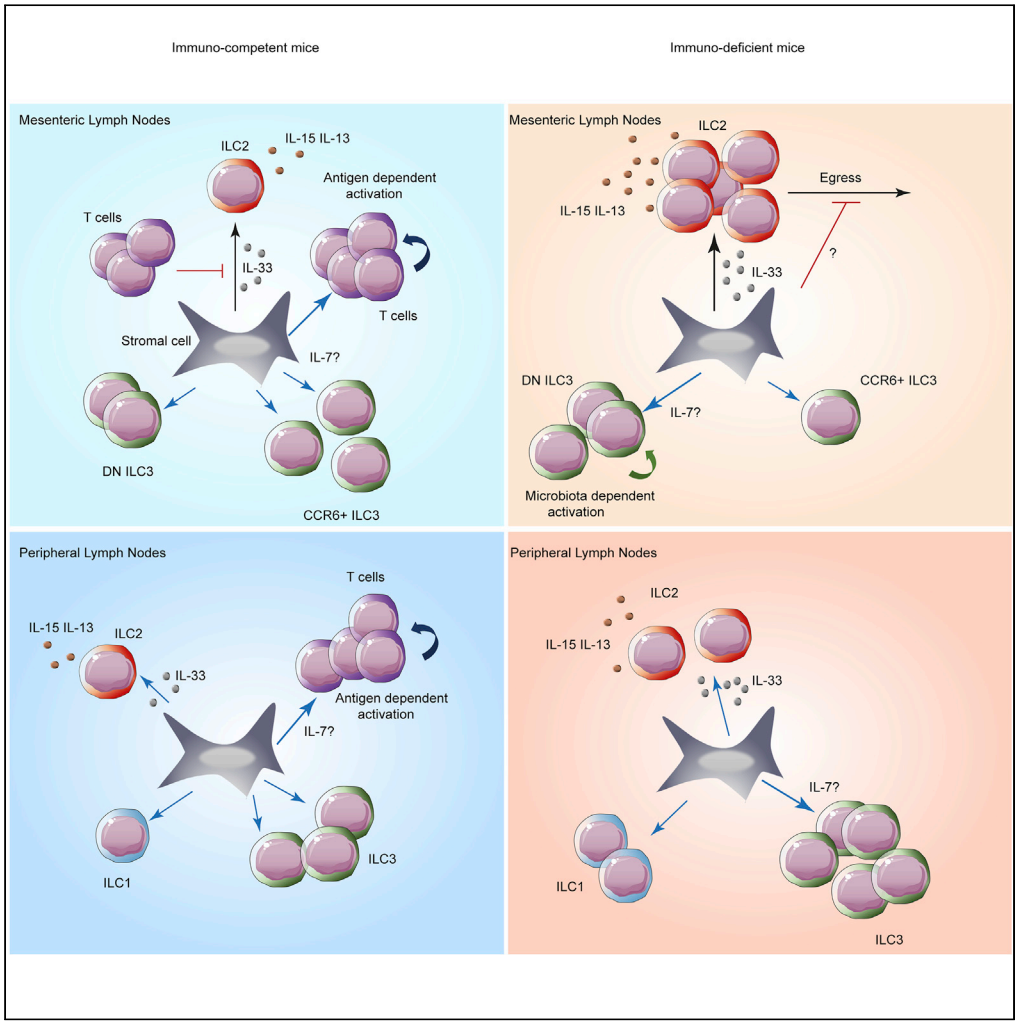

Priscillia Bresler, Emmanuel Tejerina, Jean Marie Jacob, ..., Sophie Ezine, Lucie Peduto, Marie Cherrier

marie.cherrier@inserm.fr

HIGHLIGHTS

T cells differentially regulate ILC homeostasis in PLNs and MLNs

MLNs ILC3 homeostasis is regulated by T cells in a microbiota- and age-dependent way

T cells indirectly regulate stroma-derived IL-33 in MLNs

IL-33 participates in the regulation of MLNs ILC2 homeostasis by T cells

Bresler et al., iScience 24, 102158
March 19, 2021
https://doi.org/10.1016/j.isci.2021.102158

iScience

CellPress
OPEN ACCESS

Article

T cells regulate lymph node-resident ILC populations in a tissue and subset-specific way

Priscillia Bresler,[1] Emmanuel Tejerina,[1] Jean Marie Jacob,[2,4] Agnès Legrand,[1] Véronique Quellec,[1] Sophie Ezine,[1] Lucie Peduto,[2] and Marie Cherrier[3,5,*]

SUMMARY

Innate lymphoid cells (ILCs) have been shown to be significantly affected in the small intestine lamina propria and secondary lymphoid organs (SLOs) of conventional lymphopenic mice. How ILCs are regulated by adaptive immunity in SLOs remains unclear. In T cell-deficient mice, ILC2s are significantly increased in the mesenteric lymph nodes (MLNs) at the expense of CCR6$^+$ ILC3s, which are nonetheless increased in the peripheral lymph nodes (PLNs). Here, we show that T cells regulate lymph node-resident ILCs in a tissue- and subset-specific way. First, reducing microbial colonization from birth restored CCR6$^+$ ILC3s in the MLNs of T cell-deficient mice. In contrast, T cell reconstitution resulted in the contraction of both MLNs ILC2s and PLNs ILC3s, whereas antagonizing microbial colonization from birth had no impact on these populations. Finally, the accumulation of MLNs ILC2s was partly regulated by T cells through stroma-derived IL-33.

INTRODUCTION

Innate lymphoid cells (ILCs) are critical immune cell populations that orchestrate host-commensal bacteria relationships and impact immunity, inflammation, and tissue homeostasis (Bordon, 2013) (Ebbo et al., 2017). ILCs are frequent at mucosal sites and closely associated with airways and intestinal epithelial barriers. To date, three main ILC subsets have been described based on the developmental and functional homologies with helper T cells (Spits et al., 2013). Type 1 ILCs (ILC1) express T-bet, are not cytotoxic, and produce IFNγ in the context of immune responses against intra- and extracellular pathogens. Type 2 ILCs (ILC2) express GATA-3 and produce IL-5 and IL-13 in response to epithelial cell-derived IL-25 and IL-33 upon infection with intestinal worms and respiratory viruses. They are also involved in allergies and asthma as well as adipose tissue homeostasis. Type 3 ILCs (ILC3) express the retinoic acid-related orphan receptor gamma t (RORγt). During embryogenesis, fetal ILC3s named lymphoid tissue inducer cells (LTis) initiate the formation of secondary lymphoid organs (SLOs) (Cupedo et al., 2002). After birth, IL-22 production by CCR6$^+$ ILC3s and NKp46$^+$ ILC3s participates in the protection of the gut epithelial barrier after colonization by commensal bacteria (Satoh-Takayama et al., 2008) (Song et al., 2015).

Both T cells and ILCs are involved in intestinal homeostasis and immunity. ILCs were recently shown to be redundant in both mice and humans where diverse and fully functional T cells are present (Rankin et al., 2016) (Vely et al., 2016). However, there are many situations in which this is not the case, for instance, infections, leukemia, infancy, and aging. Therefore, a dialog between T cells and ILCs is necessary to coordinate optimal immune responses in each of these situations (von Burg et al., 2015). It has been shown that ILCs have the capacity to promote and/or to modulate T cell responses toward microbiota-derived antigens (Hepworth et al., 2013) (Hepworth et al., 2015). It is possible that T cells can in turn shape the composition and the activity of ILCs, and this still needs to be investigated. RAG- and T cell-deficient mice harbor deregulated ILC populations in SLOs and in the intestine, suggesting that adaptive immunity plays an essential role in the homeostasis of these populations (Mackley et al., 2015) (Korn et al., 2014) (Mao et al., 2018). However, little is known about the functional requirements for the adaptive immune system to regulate the number, the composition, the activity, and the fitness of ILCs throughout life.

To investigate the role of T cells in the regulation of ILC homeostasis, we closely analyzed the composition and the activity of ILCs in mice that are devoid of T cells (CD3ε$^{-/-}$). We showed that constitutive T cell

[1]Institut Necker Enfants Malades, Université Paris Descartes, INSERM U1151, CNRS UMR 8253, Faculté de Médecine Necker, 156 rue de Vaugirard, 75015 Paris, France

[2]Stroma, Inflammation & Tissue Repair Unit, Institut Pasteur, Inserm U1224, Paris, France

[3]Institut Imagine, Université Paris Descartes, INSERM U1163, Laboratory of Intestinal Immunity, 24 Boulevard du Montparnasse, 75015 Paris, France

[4]Université Paris Diderot, Sorbonne Paris Cité, Paris, France

[5]Lead contact

*Correspondence: marie.cherrier@inserm.fr

https://doi.org/10.1016/j.isci.2021.102158

deficiency results in strikingly different functional and homeostatic outcomes for ILCs in a tissue-dependent manner. The fraction of CCR6$^+$ ILC3s is increased in peripheral lymph nodes (PLNs) of T cell-deficient mice after weaning, whereas the same population is drastically reduced in mesenteric lymph nodes (MLNs). Antagonizing colonization by commensal bacteria from birth restored the CCR6$^+$ ILC3s in MLNs without significant impact on this population in PLNs. In contrast, T cell adoptive transfer and microbiota-independent T cell activation significantly suppressed the accumulation of LN-resident ILCs but failed to restore LTi-like cells in MLNs. Finally, an additional layer of regulation was identified in MLNs where T cells can also reduce the accumulation of type 2 ILCs by controlling stroma-derived IL-33. These results show that the cross talk between adaptive immune cells and the tissue microenvironment is key to prevent deregulated activation of ILCs that may in turn result in immune disorders such as food allergies and inflammatory diseases.

RESULTS

Constitutive T cell deficiency results in different functional and homeostatic outcomes for ILCs depending on age and location

To dissect the role of T cells in the regulation of ILC homeostasis, the composition and the activity of ILCs were analyzed in T cell-deficient mice (CD3$\varepsilon^{-/-}$) and compared with control littermates (CD3$\varepsilon^{+/-}$) before and after weaning. ILC subsets were defined and identified using the gating strategies shown in Figures 1A and 1D.

In PLNs of weaned (8-week-old) CD3$\varepsilon^{-/-}$ mice, cell numbers were significantly increased in each ILC subset compared with control littermates (Figure 1C). Type 3 ILCs showed the most drastic increase, and this was associated with a 3-fold increase in the number of CCR6$^+$ ILC3s in the PLNs of CD3$\varepsilon^{-/-}$ mice (Figure 1F). MLNs are connected to the SILP by lymphatic vessels allowing trafficking of antigens and hematopoietic cells. Additionally, ILC1s and ILC3s were shown to traffic from the MLNs to the SILP by switching chemokine receptor expression from CCR7 to CCR9 (Kim et al., 2015). Based on previous studies reporting altered ILC populations in the SILP of lymphopenic mice and our own observations (Figures S1A–S1C), we assessed the effect of constitutive T cell deficiency on the composition of ILCs in MLNs. Although, T cell deficiency induced changes in the composition of ILCs in the MLNs of weaned CD3$\varepsilon^{-/-}$ mice (Figure 1B), it did not recapitulate those observed in the PLNs or SILP (Figures S1B). There was a 10-fold increase in the number of type 2 ILCs in the MLNs of CD3$\varepsilon^{-/-}$ mice compared with control littermates (Figure 1B), and this was reflected by an increased number of ILCs producing IL-5 and IL-13 (Figures 1G–1I) characterized as Lin$^-$ CD127$^+$ RORγt$^-$ NKp46$^-$ KLRG1$^+$ cells (Figures S2A and S2C). In contrast to PLNs (Figure 1C), the number of ILC3s was not significantly affected in the MLNs of weaned CD3$\varepsilon^{-/-}$ mice compared with CD3$\varepsilon^{-/+}$ littermates (Figure 1B), although there was a 3-fold increase in the number of NKp46$^-$ CCR6$^-$ (DN) ILC3s at the expense of CCR6$^+$ ILC3s (Figure 1E).

The composition of commensal bacterial communities colonizing the intestinal tract was shown to undergo drastic changes upon weaning. Moreover, a developmental switch in the composition and activity of SILP ILCs takes place around that time with IL-22-producing NKp46$^+$ ILC3s becoming predominant at the expense of "LTi-like" cells (CCR6$^+$ ILC3s) (Figures S1C–S1E) (Sawa et al., 2010) (Lee et al., 2011). We observed that T cell deficiency has little impact on the composition of ILCs and ILC3s in PLNs (Figures 1B and 1C) and MLNs (Figures 1E and 1F) before weaning. In contrast to what was observed in 8-week-old CD3$\varepsilon^{-/-}$ mice, the number of MLNs ILC2s also remained unaffected before weaning (Figure 1B). These observations show that T cell deficiency does not affect the homeostasis of lymph node (LN)-resident ILCs uniformly throughout ontogeny. It was recently demonstrated that the T cell-dependent containment of immuno-stimulatory commensal bacteria such as segmented filamentous bacteria is instrumental in the suppression of STAT3 activation within gut-resident type 3 ILCs after weaning (Mao et al., 2018). Therefore, we hypothesized that the transition from milk to solid food and the associated changes in the intestinal microbial community (Parigi et al., 2015) (Rogier et al., 2014) may also play a role in the regulation of ILC homeostasis by adaptive immunity in PLNs and MLNs.

Commensal bacteria differentially impact the homeostasis of PLN- and MLN-resident ILCs in the absence of T cells

To determine whether commensal bacteria promote the expansion and the activation of ILCs in the absence of T cells, a cocktail of broad-spectrum antibiotics (ampicillin, streptomycin, metronidazole, and 2% glucose in drinking water) was given from birth to T cell-deficient mice and their control littermates

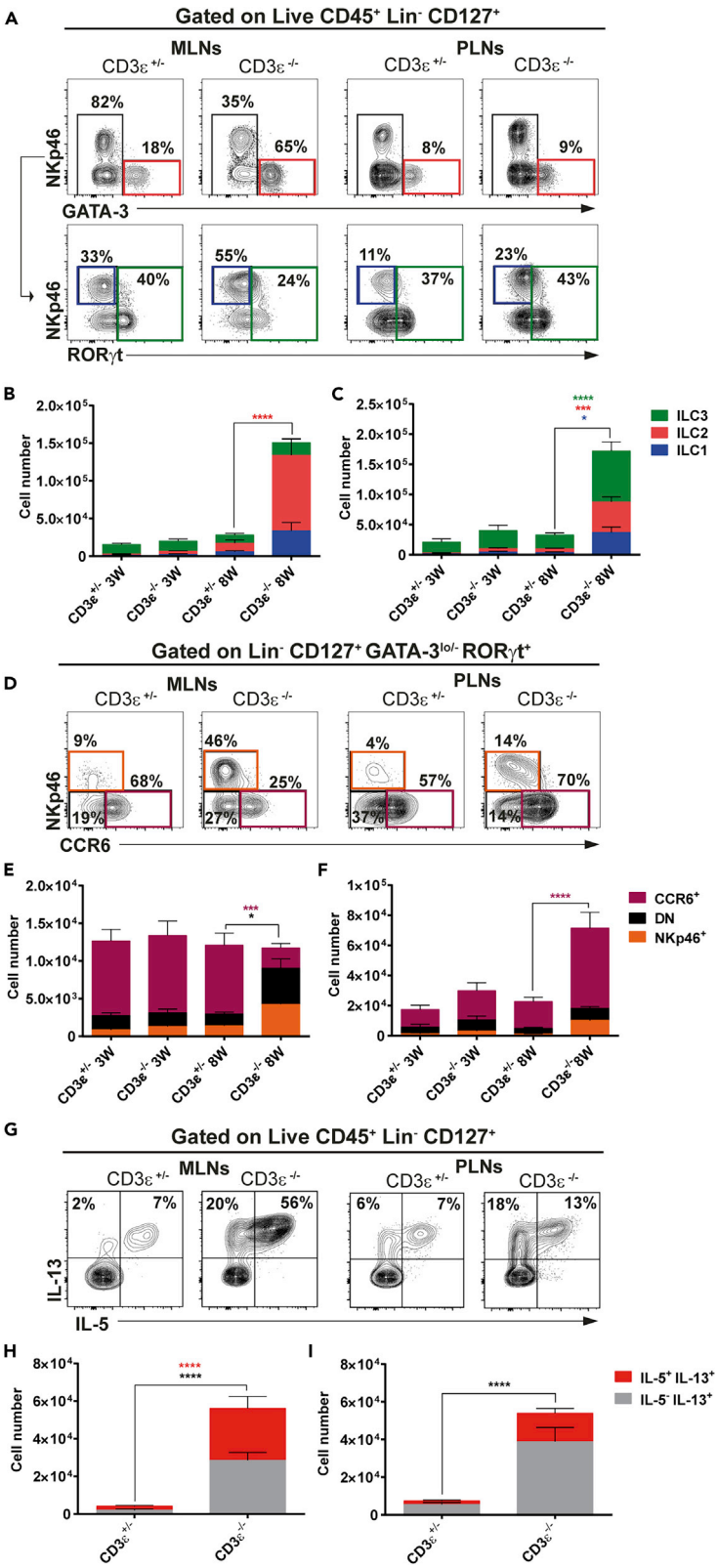
A
Gated on Live CD45+ Lin- CD127+
MLNs
PLNs
CD3ε +/-
CD3ε -/-
82%
18%
35%
65%
8%
9%
NKp46
GATA-3
33%
40%
55%
24%
11%
37%
23%
43%
NKp46
RORγt
B
Cell number
2.0x10^5
1.5x10^5
1.0x10^5
5.0x10^4
0
****
CD3ε +/- 3W
CD3ε -/- 3W
CD3ε +/- 8W
CD3ε -/- 8W
C
Cell number
2.5x10^5
2.0x10^5
1.5x10^5
1.0x10^5
5.0x10^4
0
****
***
*
ILC3
ILC2
ILC1
CD3ε +/- 3W
CD3ε -/- 3W
CD3ε +/- 8W
CD3ε -/- 8W
Gated on Lin- CD127+ GATA-3lo/- RORγt+
D
MLNs
PLNs
CD3ε +/-
CD3ε -/-
9%
68%
19%
46%
25%
27%
4%
57%
37%
14%
70%
14%
NKp46
CCR6
E
Cell number
2.0x10^4
1.5x10^4
1.0x10^4
5.0x10^3
0
***
*
CD3ε +/- 3W
CD3ε -/- 3W
CD3ε +/- 8W
CD3ε -/- 8W
F
Cell number
1x10^5
8x10^4
6x10^4
4x10^4
2x10^4
0
****
CCR6+
DN
NKp46+
CD3ε +/- 3W
CD3ε -/- 3W
CD3ε +/- 8W
CD3ε -/- 8W
G
Gated on Live CD45+ Lin- CD127+
MLNs
PLNs
CD3ε +/-
CD3ε -/-
2%
7%
20%
56%
6%
7%
18%
13%
IL-13
IL-5
H
Cell number
8x10^4
6x10^4
4x10^4
2x10^4
0
****
****
CD3ε +/-
CD3ε -/-
I
Cell number
8x10^4
6x10^4
4x10^4
2x10^4
0
****
IL-5+ IL-13+
IL-5- IL-13+
CD3ε +/-
CD3ε -/-

Figure 1. T cells regulate ILC homeostasis through distinct mechanisms depending on the ILC subtype and tissue microenvironment

(A–C) (A) Flow cytometry analysis of ILCs from the mesenteric lymph nodes (MLNs) and peripheral lymph nodes (PLNs) of 8-week-old T cell-deficient mice ($CD3\varepsilon^{-/-}$) and control littermates ($CD3\varepsilon^{+/-}$). Histograms showing cell numbers in each ILC subset in the MLNs (B) and PLNs (C) of T cell-deficient mice and control littermates before (3 weeks old $CD3\varepsilon^{-/-}$ n = 8 and $CD3\varepsilon^{+/-}$ n = 6) and after weaning (8-week-old $CD3\varepsilon^{-/-}$ n = 13 and $CD3\varepsilon^{+/-}$ n = 9).

(D) Group 3 ILCs were subdivided into three subsets according to the expression of NKp46 and CCR6: $NKp46^+$ (orange), $CCR6^+$ (purple), and $NKp46^-$ $CCR6^-$ (DN) (black).

(E and F) Histograms showing the number of cells in each ILC3 subset in MLNs and PLNs of T cell-deficient mice and control littermates before (3 weeks old $CD3\varepsilon^{-/-}$ n = 8 and $CD3\varepsilon^{+/-}$ n = 6) and after weaning (8-week-old $CD3\varepsilon^{-/-}$ n = 14 and $CD3\varepsilon^{+/-}$ n = 12).

(G) Flow cytometry analysis of type 2 cytokine production by ILCs in the MLNs and PLNs of 8-week-old T cell-deficient mice $CD3\varepsilon^{-/-}$ and control littermates $CD3\varepsilon^{+/-}$.

(H and I) Histograms showing the number of ILCs expressing IL-13 alone or in combination with IL-5 in the MLNs (H) and PLNs (I) of 8-week-old T cell-deficient mice $CD3\varepsilon^{-/-}$ (n = 16) and control littermates $CD3\varepsilon^{+/-}$ (n = 15). Statistical analysis was performed using the two-way ANOVA method and Bonferroni's multiple comparison test, with alpha = 0.05.

****$p < 0.0001$, ***$p < 0.001$, *$p < 0.05$. Data are pooled from at least 3 independent experiments. Data are represented as mean ± SEM.

See also Figures S1 and S2.

(Figure 2A). Treatment with broad-spectrum antibiotics induced a significant reduction in the cellularity of PLNs and MLNs regardless of the genotype (data not shown). Therefore, the composition and activity of ILCs were expressed as the percentage of $CD45^+$ cells rather than absolute numbers to avoid any over-estimation of the effect of antibiotics on ILC populations. ILC frequencies remained essentially unchanged in the PLNs of antibiotic-treated mice regardless of the genotype (Figures 2C, 2E, and 2G). Interestingly, antibiotic treatment from birth resulted in the complete restoration of $CCR6^+$ ILC3s (LTi-like cells) in the MLNs of T cell-deficient mice (Figure 2D). Moreover, and in line with previous observations (Korn et al., 2014) (Mao et al., 2018), the fraction of $NKp46^+$ ILC3s and IL-22 producing ILCs were drastically reduced in the SILP of antibiotic-treated T cell-deficient mice (Figures S1F–S1H). In addition, we observed that the restoration of MLNs $CCR6^+$ ILC3s was associated with a significant reduction in the percentage of $Ki67^+$ cells among DN ILC3s in MLNs, but not in PLNs of mice treated with antibiotics from birth (Figures 2H and 2I) suggesting that the microbiota may indirectly induce the proliferation of DN ILC3s at the expense of $CCR6^+$ ILC3s.

Changes in gut microbiota composition have been reported in immuno-deficient mice including T cell-deficient mice (Kawamoto et al., 2014), suggesting that not only the amount of commensal bacteria but also their content may play a dominant role in regulating MLNs ILC3 homeostasis. To address the role of microbiota composition in this process, we compared cell numbers in each ILC3 subset in the MLNs of genetically identical mice born from either T cell-deficient or competent Dam (Figures 2J and 2K). Figure 2J shows that MLNs ILC3s composition is similar in genetically identical mice regardless of the immunological and microbial status of the mother suggesting that changes in microbiota composition may not play a major role in regulating MLNs ILC3 homeostasis.

Although the fraction of type 2 ILCs and the proportion of $IL\text{-}13^+$ $IL\text{-}5^-$ ILCs were significantly reduced among MLNs $CD45^+$ cells of antibiotic-treated T cell-deficient mice (1.2% and 0.4%, respectively, in $CD3\varepsilon^{-/-}$ SPF versus 0.7% and 0.14% in $CD3\varepsilon^{-/-}$ Abx), they were still significantly increased compared with those observed in T cell-competent hosts (Figures 2B and 2F). Antibiotic treatment from birth also failed to significantly reduce the fraction of ILCs producing both IL-5 and IL-13 in the MLNs of $CD3\varepsilon^{-/-}$ mice (Figure 2F). Altogether, these observations show that commensal bacteria play a dominant role in the regulation of MLNs-resident type 3 ILCs by T cells, but have a limited impact on ILC2 homeostasis at the steady state.

T cell reconstitution reduces the accumulation of ILCs in both peripheral and mesenteric lymph nodes of T cell-deficient recipients

Next we studied whether ILC homeostasis could be restored upon T cell reconstitution after weaning. Thymic lobes from CD45.2 wild-type (WT) neonates were grafted under the kidney capsule of adult CD45.1 $CD3\varepsilon^{-/-}$ mice to mimic a progressive and physiological T cell colonization. Chimerism in MLNs was stable from 8 to 16 weeks post-graft suggesting that thymic grafts efficiently and stably reconstituted T cells in SLOs (Figure S3A). The fraction of $CD4^+$ and $CD8^+$ T cells was assessed in the MLNs 16 weeks post-graft and found to be similar to what was observed in age-matched WT mice (Figure S3B).

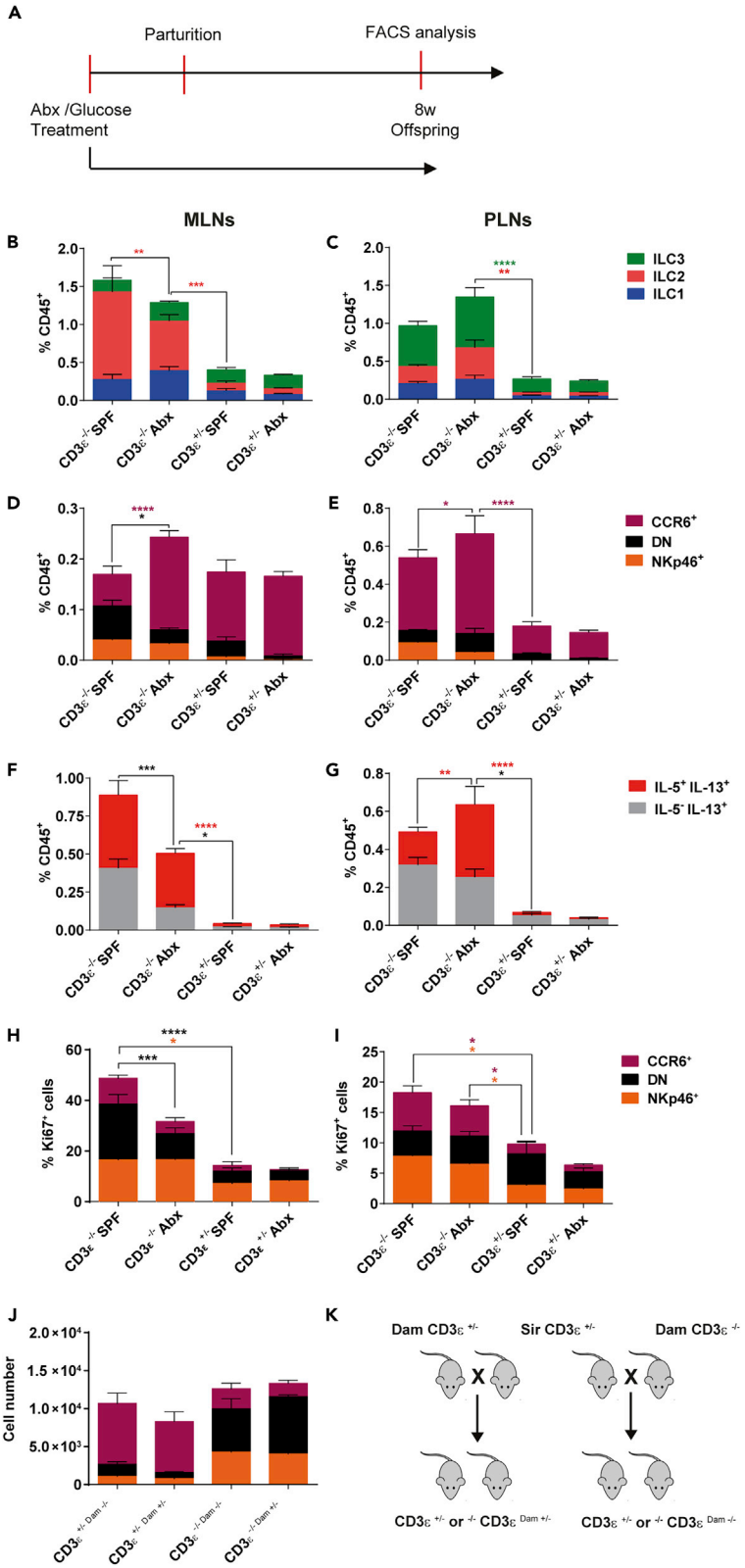
A
Parturition
FACS analysis
Abx /Glucose Treatment
8w Offspring
MLNs
PLNs
B
C
ILC3
ILC2
ILC1
% CD45+
D
E
CCR6+
DN
NKp46+
F
G
IL-5+ IL-13+
IL-5- IL-13+
H
I
% Ki67+ cells
J
Cell number
K
Dam CD3ε +/-
Sir CD3ε +/-
Dam CD3ε -/-
CD3ε +/- or -/- CD3ε Dam +/-
CD3ε +/- or -/- CD3ε Dam -/-

Figure 2. Commensal bacteria play a dominant role in the regulation of CCR6$^+$ ILC3 homeostasis in the mesenteric lymph nodes of T cell-deficient mice

(A–E) (A) Experimental procedure: T cell-deficient mice (CD3ε$^{-/-}$) and control littermates (CD3ε$^{+/-}$) were treated with a cocktail of broad-spectrum antibiotics (Abx) (ampicillin 0.5 g/L; streptomycin 1 g/L; metronidazole 0.5 g/L) in the drinking water from birth. Histograms showing the percentage of each ILC (B and C) and each ILC3 subset (D and E) among CD45$^+$ cells in MLNs (B and D) and PLNs (C and E) of 8-week-old T cell-deficient mice and control littermates treated with a cocktail of broad-spectrum antibiotics (CD3ε$^{-/-}$ Abx n = 9 and CD3ε$^{+/-}$ Abx n = 7) with 2% glucose or with 2% glucose only in the drinking water (CD3ε$^{-/-}$ SPF n = 8 and CD3ε$^{+/-}$ SPF n = 5).

(F and G) Histograms showing the percentage of ILCs expressing IL-13 alone or in combination with IL-5 among CD45$^+$ cells in the MLNs (F) and PLNs (G) of 8-week-old T cell-deficient mice and control littermates treated with a cocktail of broad-spectrum antibiotics (CD3ε$^{-/-}$ Abx n = 9 and CD3ε$^{+/-}$ Abx n = 8) or with glucose in the drinking water (CD3ε$^{-/-}$ SPF n = 8 and CD3ε$^{+/-}$ SPF n = 6).

(H and I) Percentage of Ki67$^+$ cells among ILC3 subsets in the MLNs and PLNs of the mice described above.

(J) Absolute numbers of each ILC3 subset in the MLNs of 8-week-old T cell-deficient mice and control littermates born from either SPF CD3ε$^{-/-}$ or SPF CD3ε$^{+/-}$ Dam (CD3ε$^{-/-\ Dam-/-}$ n = 8 and CD3ε$^{+/-\ Dam-/-}$ n = 6; CD3ε$^{-/-\ Dam+/-}$ n = 3 and CD3ε$^{+/-\ Dam+/-}$ n = 5).

(K) Mating strategy used to generate T cell-deficient mice and control littermates born from either CD3ε$^{-/-}$ or CD3ε$^{+/-}$ Dam. Statistical analysis was performed using the two-way ANOVA method with alpha = 0.05. ****p < 0.0001, ***p < 0.001, **p < 0.01, *p < 0.05. Data are pooled from at least 3 independent experiments. Data are represented as mean ± SEM.

See also Figure S1.

Nonetheless, significant effects on the composition of ILCs were not observed before 12 weeks post-graft (Figure S3C), indicating that newly generated T cells likely impact ILC homeostasis indirectly.

To further address which T cell subset was able to restore ILC homeostasis in the context of T cell reconstitution, CD4$^+$, CD8$^+$, and Foxp3$^+$ CD4$^+$ T cells were sorted from the PLNs and the spleen of WT or Foxp3EGFP CD45.2 mice and adoptively transferred into CD45.1 CD3ε$^{-/-}$ mice. After 12 weeks, the fraction of donor-derived cells (CD45.2$^+$) was 11% in MLNs and 15% in PLNs when CD4$^+$ or CD4$^+$ Foxp3$^+$ T cells had been injected. It was 26% in MLNs and 37% in PLNs with CD4$^+$ and CD8$^+$ T cells (Figures S3D and S3F). Staining for intracellular Ki67 in each compartment showed that a significant fraction of T cells had undergone activation and proliferation in all conditions (Figures S3E and S3G). In the MLNs, a 2-fold reduction in the number of type 2 ILCs was observed in mice reconstituted with a combination of CD4$^+$ and CD8$^+$ or CD4$^+$ T cells compared with those injected with PBS (Figures 3A and 3B). This was consistent with the 10- and 5-fold reduction in the number of ILCs secreting IL-13 and IL-5 in mice injected with CD4$^+$ and CD8$^+$ or CD4$^+$ T cells, respectively, compared with PBS injection (Figures 3A and 3F). The adoptive transfer of Foxp3$^+$ CD4$^+$ T cells significantly reduced the number of ILCs producing IL-13 and IL-5 without affecting the absolute number of type 2 ILCs (Figures 3A and 3F). In contrast to what was observed upon antibiotic treatment from birth, the adoptive transfer of T cells in adult recipients significantly reduced the fraction of PLNs ILC3s and more specifically CCR6$^+$ ILC3s (Figures 3C and 3E). In contrast, it failed to restore CCR6$^+$ ILC3s in MLNs (Figure 3D), suggesting that the developmental window during which T cells promote the maintenance of MLNs CCR6$^+$ ILC3s is restricted to earlier stages of life. Overall, these observations show that the complementation of T cell-deficient mice with CD4$^+$ T cells is sufficient to partially reduce the abundance of LN-resident ILCs and suppress the activity of MLNs ILC2s.

Microbiota is not required for the contraction of LN ILC populations upon T cell reconstitution

Polyclonal CD4$^+$ T cells undergo microbiota-dependent activation and proliferation when adoptively transferred into lymphopenic hosts (Kieper et al., 2005) (Min et al., 2005) (Feng et al., 2010). To determine if microbiota is required to regulate ILC homeostasis, CD3ε$^{-/-}$ mice were treated with antibiotics from birth and CD4$^+$ T cells were adoptively transferred at 8 weeks of age. Treatment with antibiotics was maintained for 12 weeks and ILCs were analyzed in the MLNs and PLNs. We confirmed that CD4$^+$ T cells still underwent microbiota-independent activation upon adoptive transfer by detection of intracellular Ki67 (Figure S3G). The adoptive transfer of T cells significantly reduced the fraction of IL-13- and IL-5-producing ILCs in MLNs and the frequency of CCR6$^+$ ILC3s in PLNs compared with antibiotic treatment alone (Figures 3H and 3I). However, the T cell adoptive transfer had no impact on IL-13- and IL-5-producing ILCs in PLNs (Figure 3G). These observations show that T cells can suppress the accumulation of LN-resident ILCs in a microbiota-independent way.

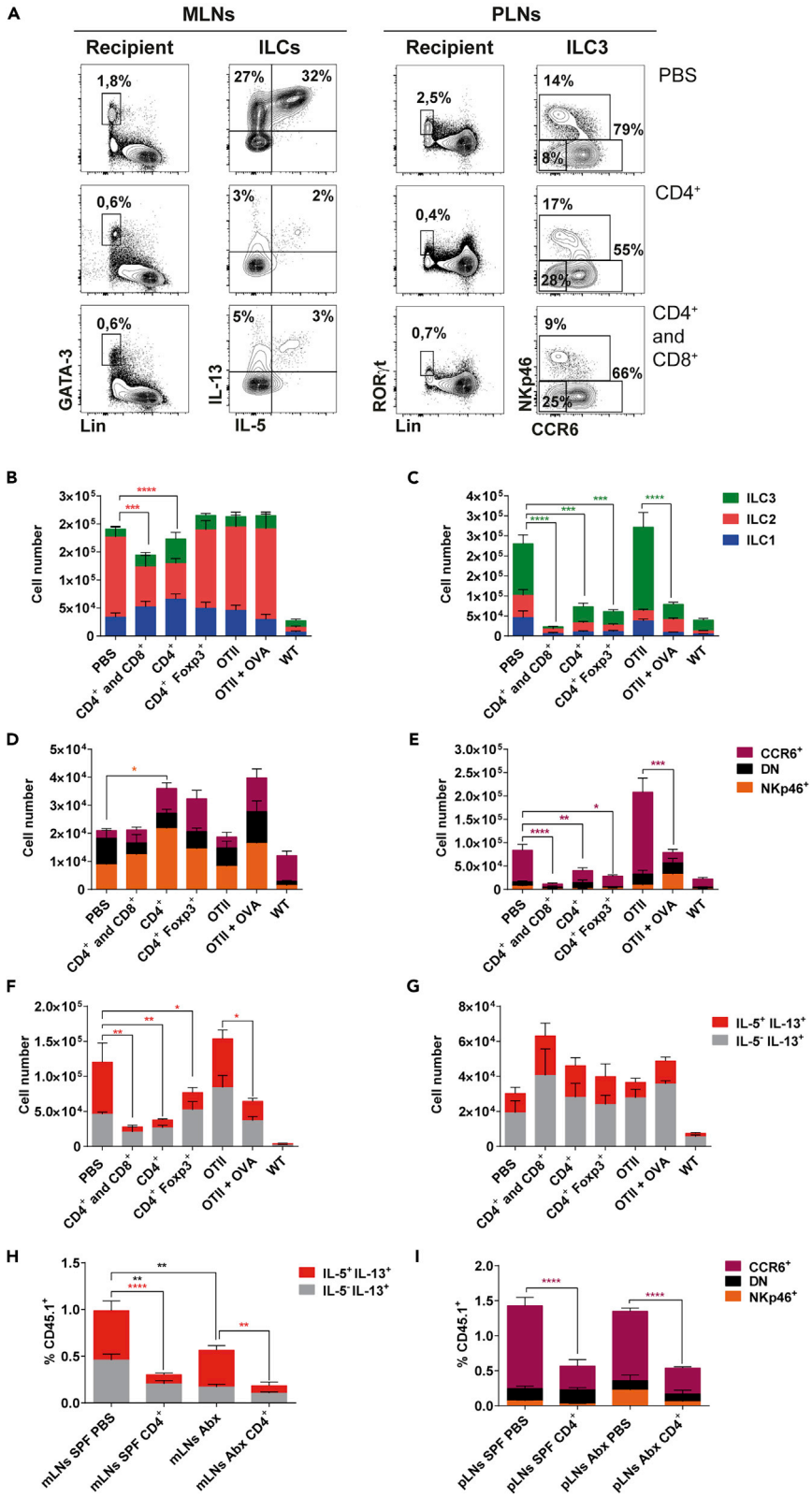
A
MLNs
PLNs
Recipient
ILCs
Recipient
ILC3
PBS
CD4+
CD4+ and CD8+
1,8%
27%
32%
2,5%
14%
79%
8%
0,6%
3%
2%
0,4%
17%
55%
28%
0,6%
5%
3%
0,7%
9%
66%
25%
GATA-3
Lin
IL-13
IL-5
RORγt
Lin
NKp46
CCR6
B
C
D
E
F
G
H
I
Cell number
ILC3
ILC2
ILC1
CCR6+
DN
NKp46+
IL-5+ IL-13+
IL-5- IL-13+
% CD45.1+
PBS
CD4+ and CD8+
CD4+
CD4+ Foxp3+
OTII
OTII + OVA
WT
mLNs SPF PBS
mLNs SPF CD4+
mLNs Abx
mLNs Abx CD4+
pLNs SPF PBS
pLNs SPF CD4+
pLNs Abx PBS
pLNs Abx CD4+

Figure 3. T cell reconstitution suppresses the expansion of LN-resident ILCs

T cell-deficient mice (CD45.1 CD3$\varepsilon^{-/-}$) received a mix of 1.5 × 10^6 $CD4^+$ and 1.5 × 10^6 $CD8^+$ T cells or 3 × 10^6 $CD4^+$ T cells or 1 × 10^6 $CD4^+$ $Foxp3^+$ T cells isolated from the peripheral lymph nodes and spleen of CD45.2 B6 mice or CD45.2 Foxp3EGFP reporter mice. When OT-II T cells were injected, mice received 3 × 10^6 $CD4^+$ T cells isolated from the peripheral lymph nodes and the spleen of CD45.2 $RAG2^{-/-}$ OT-II TCR transgenic mice. When specified, ovalbumin was added at 1.5% in the drinking water throughout the procedure. Control mice were injected with PBS. Mice were sacrificed 12 weeks following adoptive transfer, and flow cytometry analysis was performed.

(A–C) (A) Flow cytometry analysis of the fraction of Lin^- GATA-3^{hi} cells in the MLNs and of Lin^- RORγt^+ cells in the PLNs among live recipient $CD45^+$ cells in T cell-deficient mice 12 weeks after injection with PBS or 3 × 10^6 $CD4^+$ T cells or a combination of 1.5 × 10^6 $CD4^+$ and 1.5 × 10^6 $CD8^+$ T cells. Histograms showing cell numbers in each ILC subset in the MLNs and PLNs (B and C) of T cell-deficient mice injected with PBS (n = 9), $CD4^+$ and $CD8^+$ T cells (n = 6), $CD4^+$ T cells (n = 7), $Foxp3^+$ $CD4^+$ T cells (n = 8), or OT-II T cells with (n = 3) or without (n = 6) oral administration of ovalbumin, 12 weeks after the injection. WT controls are shown as a reference.

(D and E) Histograms showing the number of each ILC3 subset in the MLNs (D) and PLNs (E) of the same mice.

(F and G) Histograms showing the number of ILCs expressing IL-13 alone or in combination with IL-5 in the MLNs (F) and PLNs (G) of T cell-deficient mice treated as described above.

T cell-deficient mice (CD45.1 CD3$\varepsilon^{-/-}$) were treated with a cocktail of broad-spectrum antibiotics with 2% glucose (Abx) or 2% glucose only (SPF) in the drinking water and received 3 × 10^6 $CD4^+$ cells or PBS at 8 weeks of age. Antibiotics treatment was maintained for 12 more weeks, and flow cytometry analysis was performed.

(H) Histogram showing the frequency of ILCs expressing IL-13 alone or in combination with IL-5 among $CD45^+$ cells in the MLNs of SPF and antibiotic-treated T cell-deficient mice injected with PBS (SPF and Abx n = 8) or $CD4^+$ T cells (SPF and Abx n = 7).

(I) Histogram showing the frequency of each ILC3 subset among $CD45^+$ cells in the PLNs of the same mice. Statistical analysis was performed using two-way ANOVA method with alpha = 0.05. ****p < 0.0001, ***p < 0.001, **p < 0.01, *p < 0.05. Data are pooled from at least 3 independent experiments. Data are represented as mean ± SEM.

See also Figure S3.

Furthermore, to assess the effect of microbiota-independent $CD4^+$ T cell activation on LNs ILC frequencies, T cells derived from $RAG2^{-/-}$ OT-II TCR transgenic (tg) mice were adoptively transferred into CD3$\varepsilon^{-/-}$ mice. In contrast to polyclonal $CD4^+$ T cells, TCR tg T cells fail to expand rapidly when adoptively transferred into lymphopenic hosts in the absence of antigen (Feng et al., 2010). This was confirmed by the observation that very few cells were from donor origin in the MLNs and PLNs 12 weeks after the adoptive transfer was performed (Figure S3F). However, the addition of 1.5% ovalbumin in the drinking water induced a mild increase in the fraction of activated donor-derived T cells (Figure S3G) and the generation of a small fraction of induced Tregs in the SILP and MLNs (Figures S3H and S3I). This was correlated with a 2-fold reduction in the number of ILCs producing both IL-5 and IL-13 in mice receiving OVA compared with untreated controls (Figure 3F). However, the absolute number of type 2 ILCs remained unchanged in the MLNs as observed in mice adoptively transferred with polyclonal natural regulatory T cells (Figure 3B). In contrast, the number of $CCR6^+$ ILC3s was significantly reduced in the PLNs of mice treated with OVA (Figure 3E). Altogether, these observations show that microbiota-independent T cell activation is able to suppress the activity of MLNs type 2 ILCs and the accumulation of PLNs ILC3s during T cell reconstitution.

Stroma-derived IL-33 participates in the control of MLNs ILC2 expansion by T cells

In the MLNs, ILCs localize in the inter-follicular region (Mackley et al., 2015) and ILC3s are closely associated with marginal reticular cells (MRCs) lining the subcapsular sinus (Figures S5A and S5B), suggesting that privileged interactions with LN stromal cells are involved in ILC positioning and survival. We assessed ILC3 localization in the MLNs of T cell-deficient mice and found that their localization (Figures S4A and S4B) and association with MRCs (Figure S5A and S5B) are preserved indicating that the reduction in MLNs $CCR6^+$ ILC3s does not correlate with an altered localization of these cells within the tissue.

Specialized stromal cell subsets have been shown to play critical roles in the LN architecture and function as well as in trafficking and survival of lymphocytes, including ILCs (Kellermayer et al., 2017). Major stromal subsets were analyzed by flow cytometry in the MLNs and PLNs of T cell-deficient mice and control littermates and no significant change in their composition was observed (Figures S5C–S5E), indicating that T cell deficiency affects ILC composition without significantly changing the stromal structure.

Alarmins such as IL-25, IL-33, and TSLP have been described to promote type 2 immunity (Pulendran and Artis, 2012) (Hammad and Lambrecht, 2015). Furthermore, the gene encoding IL-33 was reported to be constitutively expressed by LNs follicular reticular cells (FRCs) (Pichery et al., 2012). To investigate the

link between T cell deficiency and the local induction of type 2 ILCs, we measured the relative mRNA expression of *Il25*, *Il33,* and *Tslp* in the distal part of the small intestine and LNs of CD3$\varepsilon^{-/-}$ mice and control littermates. *Il33* mRNA expression was increased in the MLNs of CD3$\varepsilon^{-/-}$ mice compared with control littermates, whereas *Tslp* and *Il25* expression levels remained unchanged (Figure 4A). Next we investigated whether IL-33 could promote the expansion and activation of MLNs type 2 ILCs in the absence of T cells by blocking IL-33 signaling *in vivo* using anti-IL-33R monoclonal antibody (anti-T1-ST2 mAb) (Figure 4B). The number of type 2 ILCs was measured 24 h later in the SILP and MLNs and found to be specifically and significantly reduced in the MLNs of anti-ST2-treated mice ($2.5 \pm 0.5 \times 10^4$) compared with mice injected with isotype control ($7 \pm 0.6 \times 10^4$) (Figure 4C). Accordingly, the number of ILCs producing IL-5 and IL-13 was reduced in the MLNs ($8.7 \pm 0.7 \times 10^3$ with anti-ST2 versus 2.8×10^4 with control isotype), but not in the SILP of anti-ST2-treated mice (Figures 4D and 4E). In contrast, treatment with IL-17RB and TSLP neutralizing antibodies did not induce a significant change in the numbers of ILC2s in the MLNs and SILP of T cell-deficient mice compared with isotype controls (Figures 4C–4E).

The reduction in ILC2 numbers in anti-ST2-treated mice was not correlated with reduction in cell proliferation or increased cell death as shown by Ki67 expression and Annexin V staining, respectively, (Figures 4F and 4G) suggesting that the IL-33 blockade promotes the egress of type 2 ILCs from T cell-deficient MLNs. These observations indicate that IL-33 participates in the accumulation of ILC2 in MLNs in the absence of T cells.

Il33 promoter exhibits constitutive activity in mouse lymphoid organs and the IL-33 protein is exclusively detected in LN FRCs at the steady state (Pichery et al., 2012), strongly suggesting that the main source of IL-33 in MLNs lies within CD45$^-$ cells. *Il33* mRNA expression was measured in sorted CD45$^-$ cells isolated from the MLNs of CD3$\varepsilon^{-/-}$ mice grafted with T cells, age-matched CD3$\varepsilon^{-/-}$, and control littermates (Figure 4H). We observed that CD45$^-$ stromal cells from the MLNs of CD3$\varepsilon^{-/-}$ mice express significantly higher levels of *Il33* compared with CD3$\varepsilon^{+/-}$ littermates and that these levels are restored to normal by T cell engraftment (Figure 4J). Accordingly, the number of ILC2s is restored to normal levels in the MLNs of CD3$\varepsilon^{-/-}$ mice following T cell engraftment (Figure 4I). These results suggest that T cells play a role in the regulation of IL-33 production by CD45$^-$ stromal cells residing in the MLNs.

IL-33 deficiency does not prevent the accumulation of adult bone marrow-derived ILC2s in the mesenteric lymph nodes of lymphopenic hosts

To address whether stroma-derived IL-33 is critical for the accumulation of adult bone marrow-derived ILC2s in the MLNs of lymphopenic recipients, 2×10^6 lineage-depleted bone marrow cells from 6- to 8-week-old T cell-deficient mice were injected into lethally irradiated IL-33$^{Gt/Gt}$-deficient or WT control mice (Figure 5A). Flow cytometry analysis was performed in the MLNs and SILP of the resulting chimeras 8 weeks later. The fraction of ILC2s in donor-derived cells was not significantly different in the MLNs and SILP of IL-33$^{Gt/Gt}$-deficient compared with WT recipients (Figures 5B and 5C). Accordingly, the fraction of ILCs secreting type 2 cytokines was similar in donor-derived cells isolated from the MLNs and SILP of IL-33$^{Gt/Gt}$-deficient and WT recipients (Figures 5D and 5E). These observations indicate that stroma-derived IL-33 is not strictly required for the accumulation of adult bone marrow-derived ILC2s in MLNs lacking T cells.

Altogether, these results show that IL-33 participates in the accumulation of ILC2s in the MLNs of T cell-deficient mice and that T cells directly or indirectly control IL-33 production by resident stromal cells. However, the observation that adult bone marrow-derived ILC2s do not critically rely on stroma-derived IL-33 for their accumulation in the MLNs and SILP of lymphopenic hosts suggests that additional factors compensate IL-33 deficiency. However, these observations do not rule out the possibility that IL-33 plays a critical role in the accumulation of self-renewing tissue-resident populations, but not adult bone marrow-derived ILC2s.

DISCUSSION

Recent reports have described how ILCs promote and modulate adaptive T cell responses and T cell homeostasis (Cherrier et al., 2020). The deregulation of ILC populations in lymphopenic hosts such as RAG and T cell-deficient mice suggest that adaptive immunity participates in the homeostasis of ILCs at the steady sate (Sawa et al., 2011) (Korn et al., 2014) (Mao et al., 2018). However, the mechanisms through which such regulation is achieved remain to be elucidated. We observed that T cell deficiency results in the accumulation of CCR6$^+$ ILC3s in the PLNs, whereas these cells are significantly decreased in mucosal draining LNs (Figures 1E and 1F). Similar observations have been reported in separate studies using various immuno-deficient mouse models (Withers, 2016). Here we show that in the same animal, the alteration of

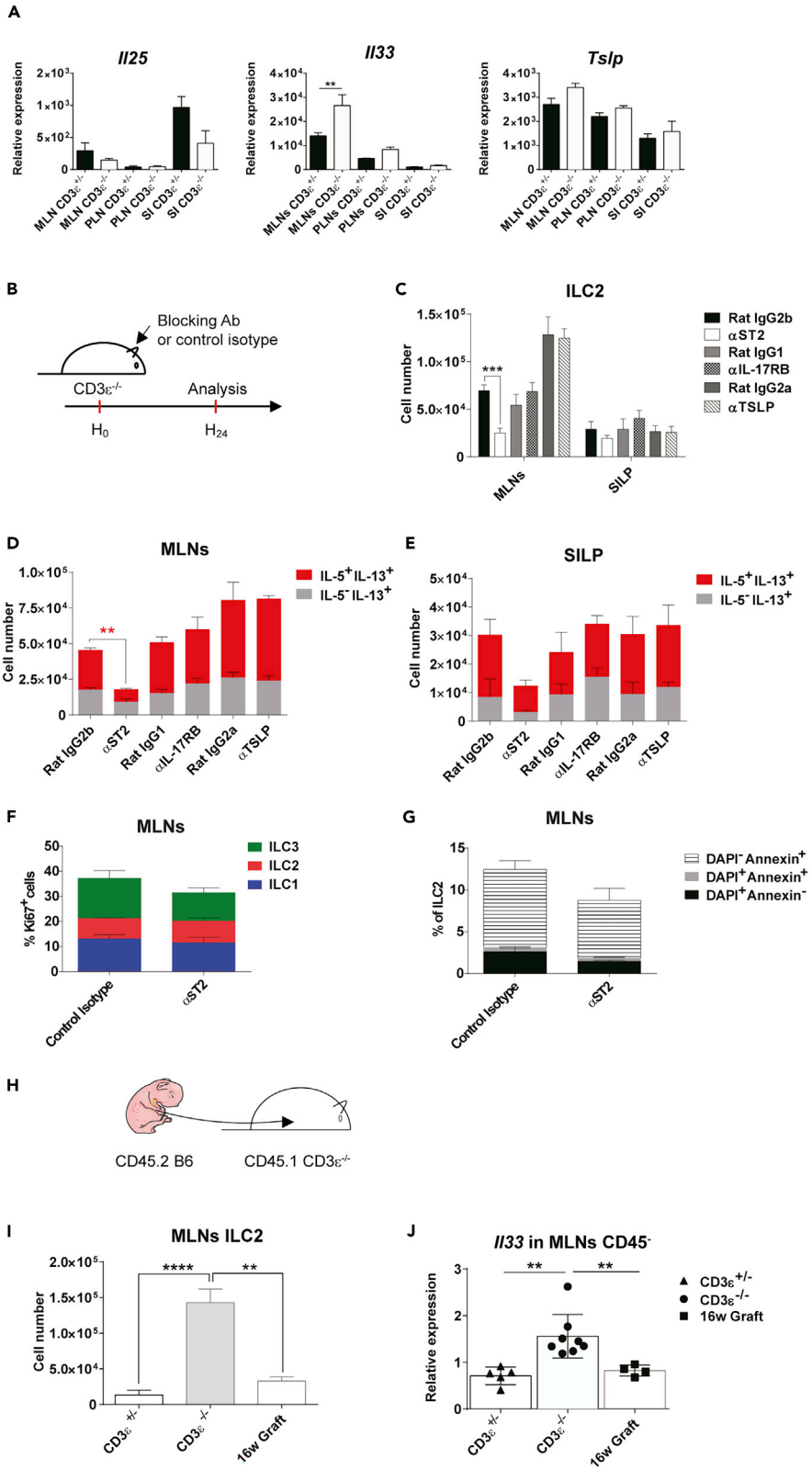
A
Il25
Il33
Tslp
Relative expression
MLN CD3ε+/-
MLN CD3ε-/-
PLN CD3ε+/-
PLN CD3ε-/-
SI CD3ε+/-
SI CD3ε-/-
MLNs CD3ε+/-
MLNs CD3ε-/-
PLNs CD3ε+/-
PLNs CD3ε-/-
SI CD3ε+/-
SI CD3ε-/-
B
Blocking Ab
or control isotype
CD3ε-/-
Analysis
H0
H24
C
ILC2
Cell number
Rat IgG2b
αST2
Rat IgG1
αIL-17RB
Rat IgG2a
αTSLP
MLNs
SILP
D
MLNs
Cell number
IL-5+IL-13+
IL-5-IL-13+
Rat IgG2b
αST2
Rat IgG1
αIL-17RB
Rat IgG2a
αTSLP
E
SILP
Cell number
IL-5+IL-13+
IL-5-IL-13+
Rat IgG2b
αST2
Rat IgG1
αIL-17RB
Rat IgG2a
αTSLP
F
MLNs
% Ki67+ cells
ILC3
ILC2
ILC1
Control Isotype
αST2
G
MLNs
% of ILC2
DAPI-Annexin+
DAPI+Annexin+
DAPI+Annexin-
Control Isotype
αST2
H
CD45.2 B6
CD45.1 CD3ε-/-
I
MLNs ILC2
Cell number
CD3ε+/-
CD3ε-/-
16w Graft
J
Il33 in MLNs CD45-
Relative expression
CD3ε+/-
CD3ε-/-
16w Graft

Figure 4. IL-33 participates in the regulation of mesenteric lymph nodes-resident ILC2 by T cells

(A) Histograms showing the relative expression of genes coding for *Il25*, *Il33,* and *Tslp* in the MLNs, PLNs, and small intestine (SI) of 8-week-old T cell-deficient mice (n = 4) and control littermates (n = 4). Statistical analysis was performed using the t test method and Mann-Whitney comparison test, with alpha = 0.05. **p < 0.01. Data are represented as mean ± SEM.

(B) Experimental procedure: Age-matched CD3ε$^{-/-}$ mice were treated with blocking antibodies directed against ST2 (n = 5), IL-17RB (n = 5), and TSLP (n = 5) or control isotype (Rat IgG2b, IgG1, and IgG2a respectively, n = 5 each) and sacrificed 24 h later for flow cytometry analysis.

(C) Histogram showing the number of ILC2s in the MLNs and SILP in each experimental condition.

(D and E) Histograms showing the number of ILCs producing IL-13 alone or in combination with IL-5 in the MLNs and SILP of the same mice.

(F) Histogram showing the percentage of Ki67^{+} cells in each ILC subset from the MLNs of mice treated with anti-ST2 or control isotype.

(G) Histogram showing the percentage of cells positive for Annexin V, DAPI, or both among MLNs ILC2. Statistical analysis was performed using the two-way ANOVA method with alpha = 0.05. ***p < 0.001, **p < 0.01. Data are from one representative experiment out of two. Data are represented as mean ± SEM.

(H) Experimental procedure: thymic lobes from CD45.2 C57BL/6 neonates were grafted under the kidney capsule of 8-week-old CD45.1 CD3ε$^{-/-}$ mice, and recipients were sacrificed 16 weeks later. Flow cytometry analysis was performed on MLNs CD45^{+} cells (I), and CD45^{-} cells were isolated and sorted for qPCR analysis (J).

(I) Histogram showing the number of ILC2s in the MLNs of T cell-deficient mice grafted with neonatal thymic lobes from CD45.2 B6 mice (n = 8), aged-matched T cell-deficient mice (n = 8), and control littermates (n = 8). Statistical analysis was performed using the two-way ANOVA method with alpha = 0.05. ****p < 0.0001, **p < 0.01. Data are pooled from 3 independent experiments. Data are represented as mean ± SEM.

(J) Relative *Il33* mRNA expression in CD45^{-} cells sorted from the MLNs of T cell-deficient mice grafted with neonatal thymic lobes (n = 8) and age-matched T cell-deficient mice (n = 8) and control littermates (n = 8). Statistical analysis was performed using the two-way ANOVA method with alpha = 0.05. **p < 0.01. Data are pooled from 3 independent experiments. Data are represented as mean ± SEM.

See also Figures S4 and S5.

ILC homeostasis by T cell deficiency differs between peripheral and mucosa-associated lymphoid organs, strongly suggesting that T cell-mediated regulation of ILC homeostasis relies on tissue-specific environmental factors. These alterations are only observed after weaning suggesting a role for the gut microbiota (Figures 1B and S1B). Additionally, we confirm that microbiota-dependent T cell activation is necessary to regulate SILP type 3 ILCs in the context of T cell constitution (Figures S1I–S1K) (Korn et al., 2014).

We showed that interactions between the TCR and its cognate antigen are necessary to suppress lymphoid tissue-resident ILCs. Indeed, adoptively transferred T cells specific for a peptide derived from ovalbumin (RAG2$^{-/-}$ OT-II) were able to efficiently suppress the production of type 2 cytokines by MLNs-resident ILCs of T cell-deficient recipients in the presence of antigen (Figure 3F). Furthermore, polyclonal T cell activation resulted in a reduction in the number of type 2 ILCs in MLNs (Figures 3B and 3F) and of type 3 ILCs in PLNs (Figures 3C and 3E). Activated T cells that rapidly expand in conditions of lymphopenia (Feng et al., 2010) may therefore outcompete lymphoid tissue-resident ILCs for limited amounts of survival factors such as IL-2 and/or IL-7 (Schmutz et al., 2009) (Martin et al., 2017).

We observed that the number of each ILC subset is increased in the PLNs (Figure 1C), whereas type 2 ILCs are specifically induced in the MLNs of T cell-deficient mice (Figures 1B and 1E) (Figures S2A–S2D). Stromal and dendritic cells derived from the MLNs of immuno-competent mice were shown to promote the differentiation of peripheral Tregs and the induction of CCR9 and α4β7 expression by activated T cells (Iwata et al., 2004). Moreover, CCR6^{+} ILC3s are located in the inter-follicular space of MLNs creating a unique environment for antigen presentation and T cell activation (Mackley et al., 2015) (Figure S4). These observations strongly suggest that tissue-specific interactions take place between ILCs and LN stromal cells within the mucosal draining LNs. It is unclear to what extent constitutive T cell deficiency affects the non-hematopoietic microenvironment of ILCs within these lymphoid tissues. We neither observed significant alterations in the location of type 3 ILCs within MLNs of T cell-deficient mice compared with control littermates (Figures S4 and S5) nor did we detect significant alterations in the composition of MLNs and PLNs stromal cell subsets in the absence of T cells (Figure S5). However, when measuring the expression of genes encoding alarmins in whole lymphoid tissues, we detected increased *IL-33* mRNA expression in the MLNs of T cell-deficient mice (Figure 4A). Neutralizing IL-33 *in vivo* efficiently reduced the number of type 2 ILCs in the MLNs of T cell-deficient mice (Figures 4C and 4D), confirming a role for this alarmin in the accumulation of these cells. The same could be observed upon T cell reconstitution (Figure 4I). Indeed, *IL-33* gene expression was induced in MLNs CD45^{-} cells of T cell-deficient mice and down-regulated

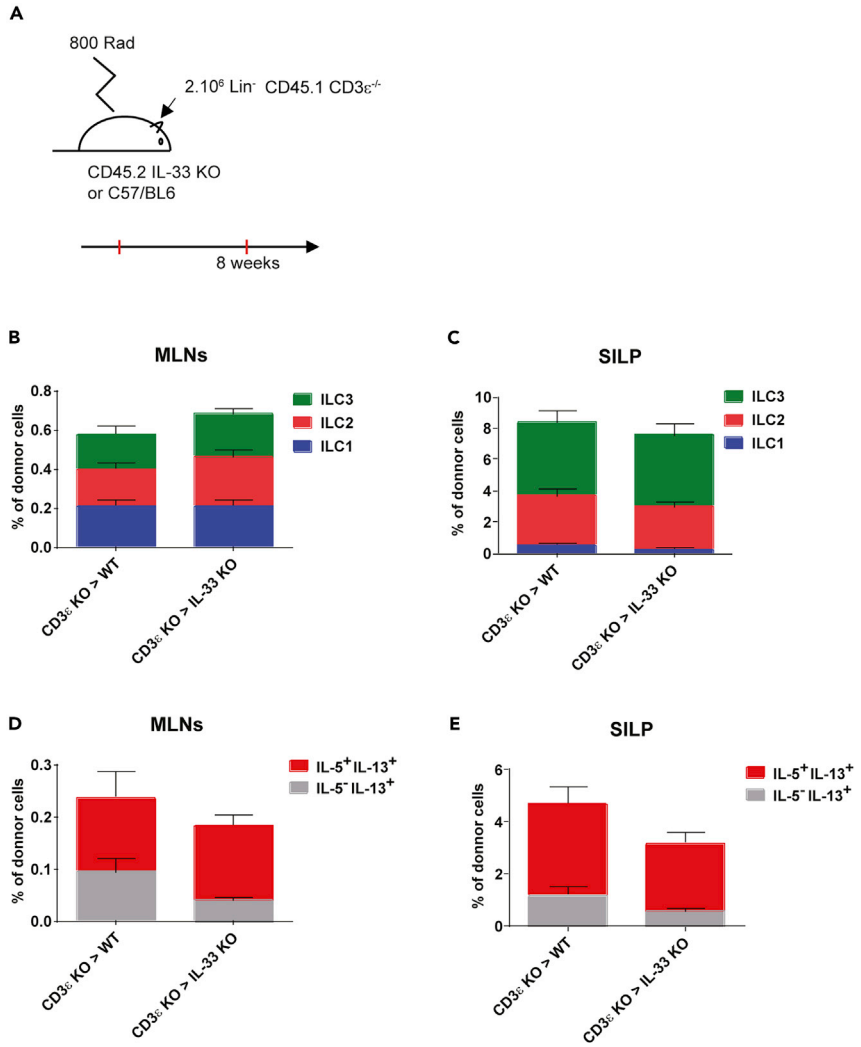

Figure 5. Stromal IL-33 is not required for the accumulation of bone marrow-derived ILC2s in the mesenteric lymph nodes and small intestine lamina propria of lymphopenic hosts

(A–C) (A) Experimental procedure: 8-week-old IL-33$^{Gt/Gt}$-deficient mice or wild-type mice were lethally irradiated and injected with 2 × 10^6 bone marrow cells isolated from CD3ε$^{-/-}$ mice and depleted from Lineage$^+$ cells. Histograms showing the percentage of each ILC subset in donor-derived cells 8 weeks after bone marrow transfer in the MLNs (B) and SILP (C) of IL-33$^{Gt/Gt}$-deficient (n = 8) and wild-type recipients (n = 8).

(D and E) Histograms showing the fraction of ILCs producing IL-13 alone or in combination with IL-5 in MLNs and SILP donor-derived cells of the same mice. Statistical analysis was performed using the t test method and Mann-Whitney comparison test, with alpha = 0.05. Data are pooled from two independent experiments. Data are represented as mean ± SEM.

upon T cell reconstitution, suggesting that T cells control *Il33* gene expression by MLNs stromal cells (Figure 4J). Finally, we did not find evidence of a critical role for stromal IL-33 in the accumulation of bone marrow-derived ILC2s in the MLNs of adult lymphopenic hosts (Figure 5). Therefore, the differential effect of T cell deficiency on ILC2 numbers in MLNs versus PLNs is only partially dependent on IL-33. Colonization of non-lymphoid tissues by ILC2s was recently shown to take place during the perinatal period with limited input from the adult bone marrow in the renewal of these populations later in life (Schneider et al., 2019). Although MLNs were not specifically investigated in this study, it is reasonable to assume that ILC2s follow the same rules in this compartment. IL-33 was also shown to play an essential role in licensing thermogenesis during the perinatal period (Odegaard et al., 2016), suggesting that its importance may fluctuate throughout life. Therefore, our observations do not rule out a critical role for IL-33 in the accumulation of self-renewing tissue-resident ILC2 in the MLNs of T cell-deficient mice before and during adulthood. Overall, our investigations dissect the diversity of mechanisms

through which adaptive immunity shapes the composition, the abundance, and the activity of innate lymphoid cells in lymphoid tissues at the steady state. In doing so, we described a functional interaction between T cells and stromal cells controlling ILC homeostasis in mucosal draining LNs.

Limitations of the study

Mice used in this study were kept on the C57BL/6 genetic background, and we did not investigate whether the same observations apply to other genetic backgrounds such as BALB/c mice. We did not have access to germ-free immuno-deficient mice to investigate the role of the microbiota in our study.

Resource availability

Lead contact

Marie Cherrier, Institut Imagine, Université Paris Descartes, INSERM U1163, Laboratory of Intestinal Immunity, 24 Boulevard du Montparnasse, 75015 Paris Email (marie.cherrier@inserm.fr), Phone number: +33(1) 42754274.

Materials availability

This study did not generate new unique reagents.

Data and code availability

This study did not generate/analyze datasets/codes.

METHODS

All methods can be found in the accompanying Transparent methods supplemental file.

SUPPLEMENTAL INFORMATION

Supplemental information can be found online at https://doi.org/10.1016/j.isci.2021.102158.

ACKNOWLEDGMENTS

We thank Gerard Eberl for kindly providing Rorc(γt)-Gfp^{TG} mice. We thank Andrew MacKenzie for kindly providing anti IL-17RB monoclonal antibody. We thank Jean Philippe Girard for kindly providing IL-33$^{Gt/Gt}$-deficient mice. We thank Jerome Mégret and Corinne Cordier from the Structure Fédérative de Recherche Cell sorting Facility for technical help and support. We thank Rachid Zoubairi, Thomas Ferré, Amandine Mainreck, and Nadia Elganfoud from the animal facility for handling mice and managing mouse breeding. P.B. was supported by a fellowship from the French Ministry of Higher Education, Research and Innovation. M.C. received financial support from "Association François Aupetit," a non-profit association dedicated to help and support patients suffering from inflammatory bowel diseases. S.E. and M.C. received support from "Fondation pour la Recherche Médicale" and "Institut National de la Recherche Médicale (INSERM)."

AUTHOR CONTRIBUTIONS

P.B. performed and designed experiments and participated in the preparation of the manuscript. E.T. and A.L. performed experiments, and E.T. handled mouse experimental procedures. V.Q. performed mouse genotyping. S.E. designed experiments, performed thymic lobes graft under the kidney capsule, and secured funding. L.P., J.M.J., and M.C. designed experiments on lymph nodes stromal cells, and J.M.J. performed those experiments. M.C. designed and performed experiments, wrote the manuscript, and secured funding.

DECLARATION OF INTERESTS

The authors have no conflict of interest to declare.

Received: April 20, 2020
Revised: December 15, 2020
Accepted: February 3, 2021
Published: March 19, 2021

REFERENCES

Bordon, Y. (2013). Mucosal immunology: ILCs broker peace deals in the gut. Nat. Rev. Immunol. *13*, 473.

von Burg, N., Turchinovich, G., and Finke, D. (2015). Maintenance of immune homeostasis through ILC/T cell interactions. Front. Immunol. *6*, 416.

Cherrier, M., Ramachandran, G., and Golub, R. (2020). The interplay between innate lymphoid cells and T cells. Mucosal Immunol. *13*, 732–742.

Cupedo, T., Kraal, G., and Mebius, R.E. (2002). The role of CD45+CD4+CD3- cells in lymphoid organ development. Immunol. Rev. *189*, 41–50.

Ebbo, M., Crinier, A., Vély, F., and Vivier, E. (2017). Innate lymphoid cells: major players in inflammatory diseases. Nat. Rev. Immunol. *17*, 665–678.

Feng, T., Wang, L., Schoeb, T.R., Elson, C.O., and Cong, Y. (2010). Microbiota innate stimulation is a prerequisite for T cell spontaneous proliferation and induction of experimental colitis. J. Exp. Med. *207*, 1321–1332.

Hammad, H., and Lambrecht, B.N. (2015). Barrier epithelial cells and the control of type 2 immunity. Immunity *43*, 29–40.

Hepworth, M.R., Monticelli, L.A., Fung, T.C., Ziegler, C.G.K., Grunberg, S., Sinha, R., Mantegazza, A.R., Ma, H.-L., Crawford, A., Angelosanto, J.M., et al. (2013). Innate lymphoid cells regulate CD4+ T-cell responses to intestinal commensal bacteria. Nature *498*, 113–117.

Hepworth, M.R., Fung, T.C., Masur, S.H., Kelsen, J.R., McConnell, F.M., Dubrot, J., Withers, D.R., Hugues, S., Farrar, M.A., Reith, W., et al. (2015). Group 3 innate lymphoid cells mediate intestinal selection of commensal bacteria–specific CD4+ T cells. Science *348*, 1031–1035.

Iwata, M., Hirakiyama, A., Eshima, Y., Kagechika, H., Kato, C., and Song, S.-Y. (2004). Retinoic acid imprints gut-homing specificity on T cells. Immunity *21*, 527–538.

Kawamoto, S., Maruya, M., Kato, L.M., Suda, W., Atarashi, K., Doi, Y., Tsutsui, Y., Qin, H., Honda, K., Okada, T., et al. (2014). Foxp3+ T cells regulate immunoglobulin A selection and facilitate diversification of bacterial species responsible for immune homeostasis. Immunity *41*, 152–165.

Kellermayer, Z., Vojkovics, D., and Balogh, P. (2017). Innate lymphoid cells and their stromal microenvironments. Immunol. Lett. *189*, 3–9.

Kieper, W.C., Troy, A., Burghardt, J.T., Ramsey, C., Lee, J.Y., Jiang, H.-Q., Dummer, W., Shen, H., Cebra, J.J., and Surh, C.D. (2005). Recent immune status determines the source of antigens that drive homeostatic T cell expansion. J. Immunol. *174*, 3158–3163.

Kim, M.H., Taparowsky, E.J., and Kim, C.H. (2015). Retinoic acid differentially regulates the migration of innate lymphoid cell subsets to the gut. Immunity *43*, 107–119.

Korn, L.L., Thomas, H.L., Hubbeling, H.G., Spencer, S.P., Sinha, R., Simkins, H.M.A., Salzman, N.H., Bushman, F.D., and Laufer, T.M. (2014). Conventional CD4+ T cells regulate IL-22 producing intestinal innate lymphoid cells. Mucosal Immunol. *7*, 1045–1057.

Lee, J.S., Cella, M., McDonald, K.G., Garlanda, C., Kennedy, G.D., Nukaya, M., Mantovani, A., Kopan, R., Bradfield, C.A., Newberry, R.D., et al. (2011). AHR drives the development of gut ILC22 cells and postnatal lymphoid tissues via pathways dependent on and independent of Notch. Nat. Immunol. *13*, 144–151.

Mackley, E.C., Houston, S., Marriott, C.L., Halford, E.E., Lucas, B., Cerovic, V., Filbey, K.J., Maizels, R.M., Hepworth, M.R., Sonnenberg, G.F., et al. (2015). CCR7-dependent trafficking of RORgamma(+) ILCs creates a unique microenvironment within mucosal draining lymph nodes. Nat. Commun. *6*, 5862.

Mao, K., Baptista, A.P., Tamoutounour, S., Zhuang, L., Bouladoux, N., Martins, A.J., Huang, Y., Gerner, M.Y., Belkaid, Y., and Germain, R.N. (2018). Innate and adaptive lymphocytes sequentially shape the gut microbiota and lipid metabolism. Nature *554*, 255–259.

Martin, C.E., Spasova, D.S., Frimpong-Boateng, K., Kim, H.-O., Lee, M., Kim, K.S., and Surh, C.D. (2017). Interleukin-7 availability is maintained by a hematopoietic cytokine sink comprising innate lymphoid cells and T cells. Immunity *47*, 171–182.

Min, B., Yamane, H., Hu-Li, J., and Paul, W.E. (2005). Spontaneous and homeostatic proliferation of CD4 T cells are regulated by different mechanisms. J. Immunol. *174*, 6039–6044.

Odegaard, J.I., Lee, M.-W., Sogawa, Y., Bertholet, A.M., Locksley, R.M., Weinberg, D.E., Kirichok, Y., Deo, R.C., and Chawla, A. (2016). Perinatal licensing of thermogenesis by IL-33 and ST2. Cell *166*, 841–854.

Parigi, S.M., Eldh, M., Larssen, P., Gabrielsson, S., and Villablanca, E.J. (2015). Breast milk and solid food shaping intestinal immunity. Front. Immunol. *6*, 415.

Pichery, M., Mirey, E., Mercier, P., Lefrancais, E., Dujardin, A., Ortega, N., and Girard, J.-P. (2012). Endogenous IL-33 is highly expressed in mouse epithelial barrier tissues, lymphoid organs, brain, embryos, and inflamed tissues: in situ analysis using a novel Il-33–LacZ gene trap reporter strain. J. Immunol. *188*, 3488–3495.

Pulendran, B., and Artis, D. (2012). New paradigms in type 2 immunity. Science *337*, 431–435.

Rankin, L.C., Girard-Madoux, M.J.H., Seillet, C., Mielke, L.A., Kerdiles, Y., Fenis, A., Wieduwild, E., Putoczki, T., Mondot, S., Lantz, O., et al. (2016). Complementarity and redundancy of IL-22-producing innate lymphoid cells. Nat. Immunol. *17*, 179–186.

Rogier, E.W., Frantz, A.L., Bruno, M.E.C., Wedlund, L., Cohen, D.A., Stromberg, A.J., and Kaetzel, C.S. (2014). Secretory antibodies in breast milk promote long-term intestinal homeostasis by regulating the gut microbiota and host gene expression. Proc. Natl. Acad. Sci. U S A *111*, 3074–3079.

Satoh-Takayama, N., Vosshenrich, C.A., Lesjean-Pottier, S., Sawa, S., Lochner, M., Rattis, F., Mention, J.J., Thiam, K., Cerf-Bensussan, N., Mandelboim, O., et al. (2008). Microbial flora drives interleukin 22 production in intestinal NKp46+ cells that provide innate mucosal immune defense. Immunity *29*, 958–970.

Sawa, S., Cherrier, M., Lochner, M., Satoh-Takayama, N., Fehling, H.J., Langa, F., Di Santo, J.P., and Eberl, G. (2010). Lineage relationship analysis of RORgammat+ innate lymphoid cells. Science *330*, 665–669.

Sawa, S., Lochner, M., Satoh-Takayama, N., Dulauroy, S., Berard, M., Kleinschek, M., Cua, D., Di Santo, J.P., and Eberl, G. (2011). RORgammat(+) innate lymphoid cells regulate intestinal homeostasis by integrating negative signals from the symbiotic microbiota. Nat. Immunol. *12*, 320–326.

Schmutz, S., Bosco, N., Chappaz, S., Boyman, O., Acha-Orbea, H., Ceredig, R., Rolink, A.G., and Finke, D. (2009). Cutting edge: IL-7 regulates the peripheral pool of adult RORγ^+ lymphoid tissue inducer cells. J. Immunol. *183*, 2217–2221.

Schneider, C., Lee, J., Koga, S., Ricardo-Gonzalez, R.R., Nussbaum, J.C., Smith, L.K., Villeda, S.A., Liang, H.-E., and Locksley, R.M. (2019). Tissue-resident Group 2 innate lymphoid cells differentiate by layered ontogeny and in situ perinatal priming. Immunity *50*, 1425–1438.

Song, C., Lee, J.S., Gilfillan, S., Robinette, M.L., Newberry, R.D., Stappenbeck, T.S., Mack, M., Cella, M., and Colonna, M. (2015). Unique and redundant functions of NKp46+ ILC3s in models of intestinal inflammation. J. Exp. Med. *212*, 1869–1882.

Spits, H., Artis, D., Colonna, M., Diefenbach, A., Di Santo, J.P., Eberl, G., Koyasu, S., Locksley, R.M., McKenzie, A.N.J., Mebius, R.E., et al. (2013). Innate lymphoid cells–a proposal for uniform nomenclature. Nat. Rev. Immunol. *13*, 145–149.

Vely, F., Barlogis, V., Vallentin, B., Neven, B., Piperoglou, C., Perchet, T., Petit, M., Yessaad, N., Touzot, F., Bruneau, J., et al. (2016). Evidence of innate lymphoid cell redundancy in humans. Nat. Immunol. *11*, 1291–1299.

Withers, D.R. (2016). Innate lymphoid cell regulation of adaptive immunity. Immunology *149*, 123–130.

iScience, Volume *24*

Supplemental information

T cells regulate lymph node-resident ILC populations in a tissue and subset-specific way

Priscillia Bresler, Emmanuel Tejerina, Jean Marie Jacob, Agnès Legrand, Véronique Quellec, Sophie Ezine, Lucie Peduto, and Marie Cherrier

Supplementary Figure 1

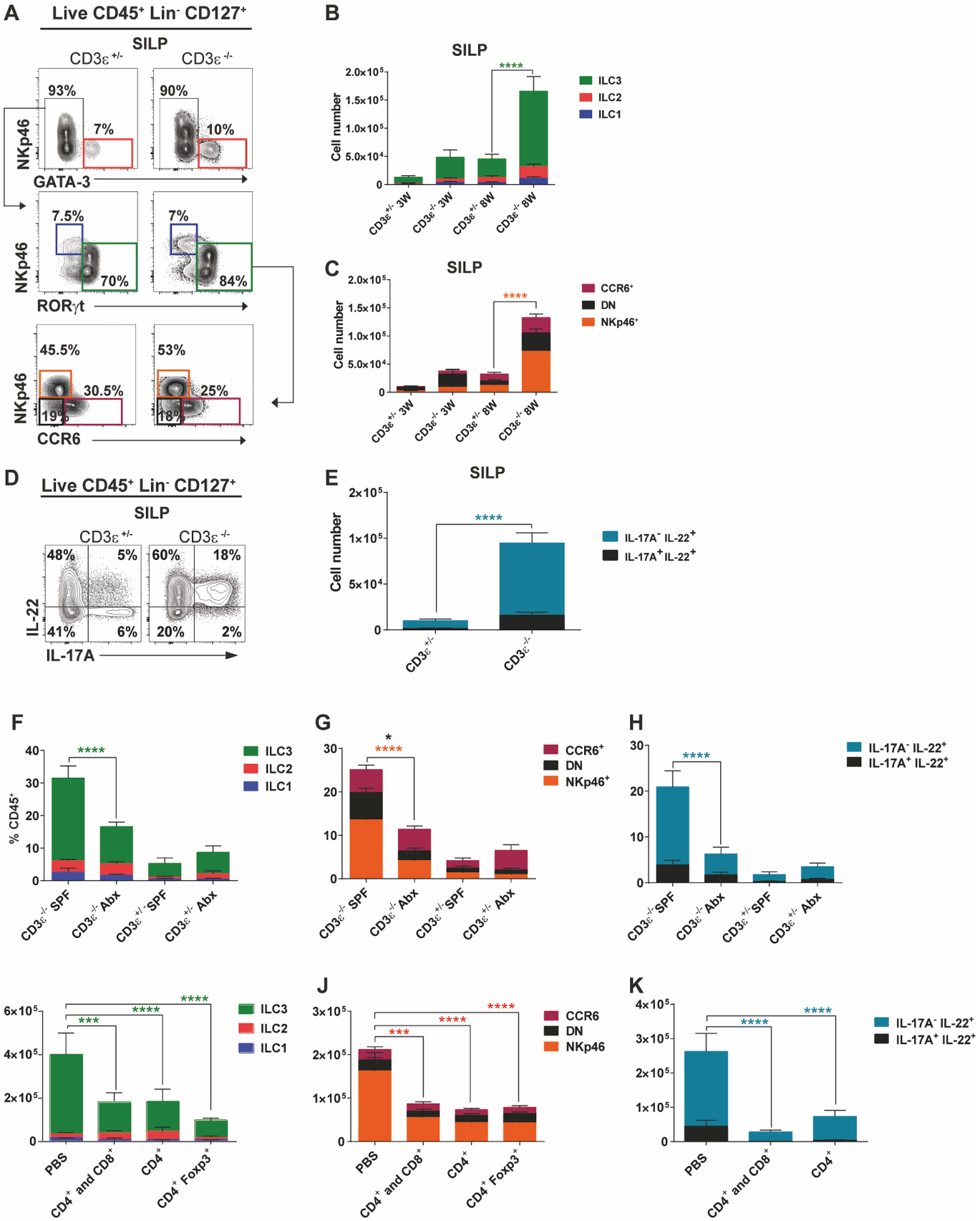

Supplementary Figure 2

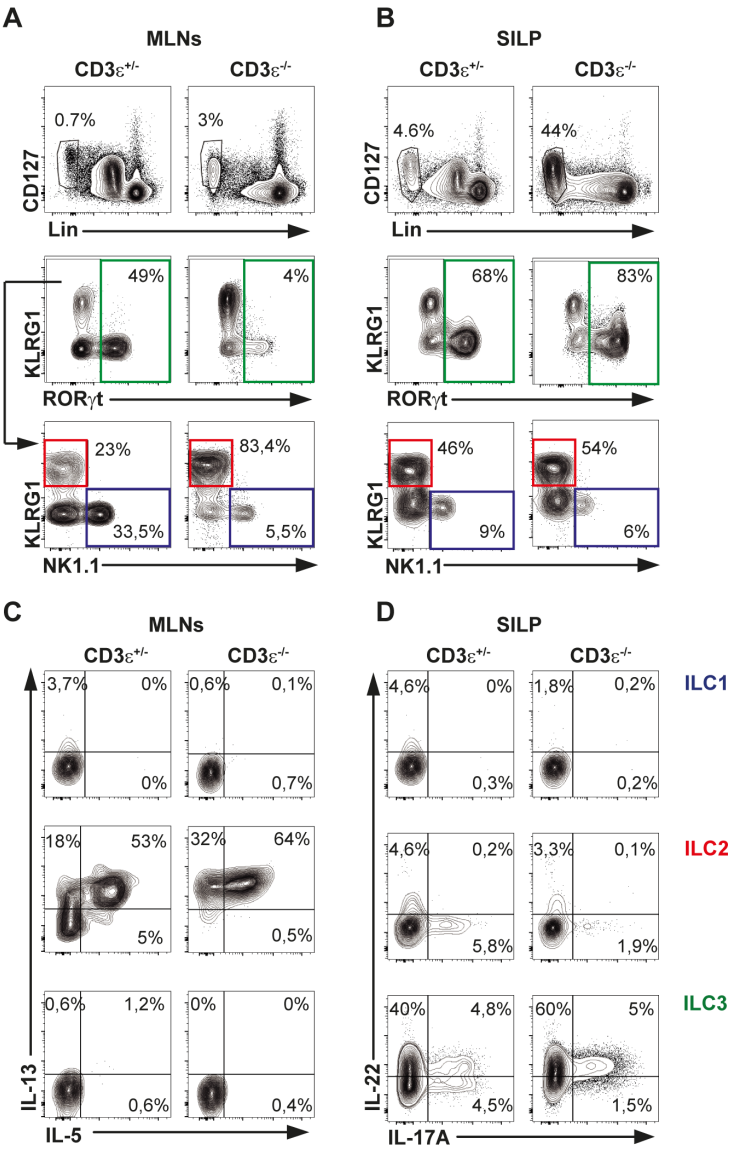

Supplementary Figure 3

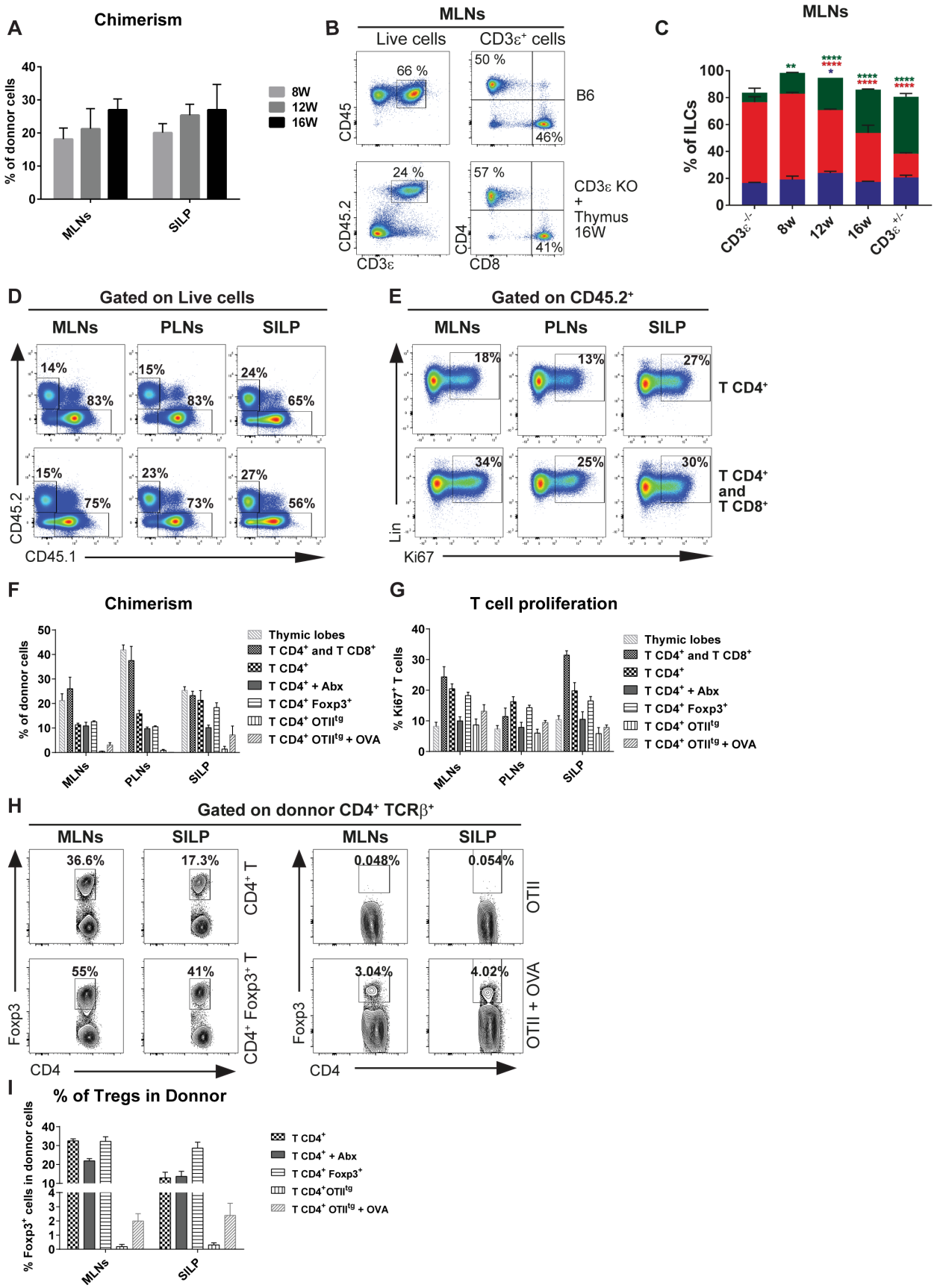

Supplementary Figure 4

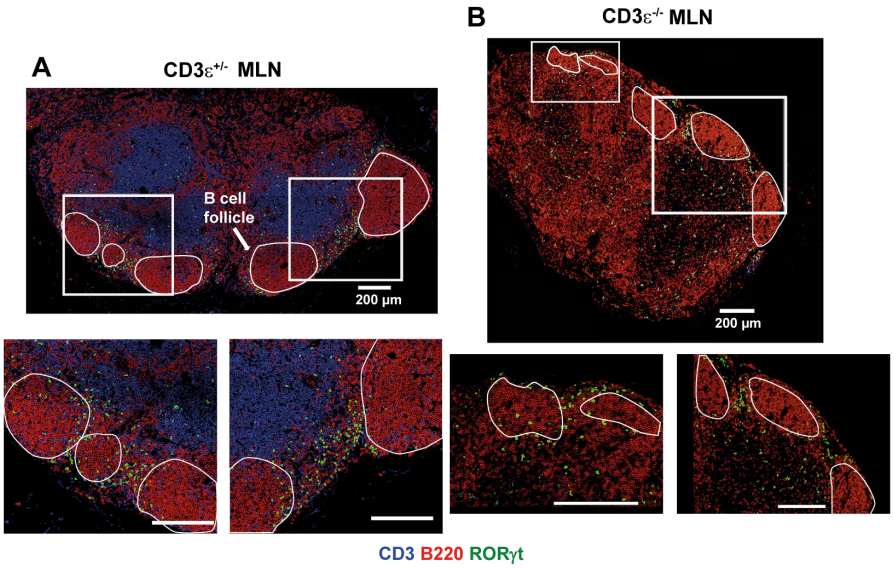

Supplementary Figure 5

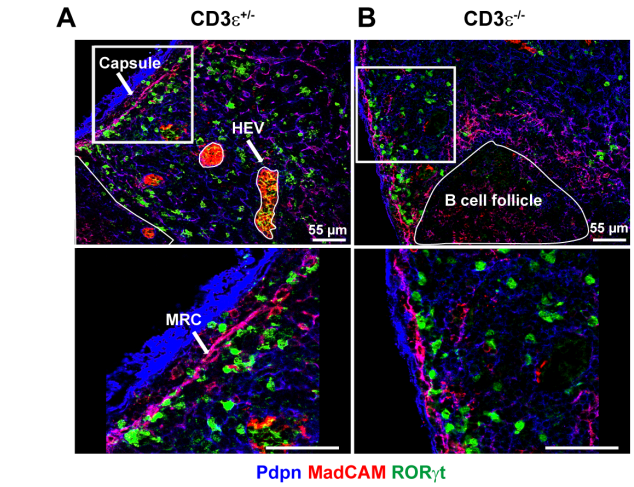

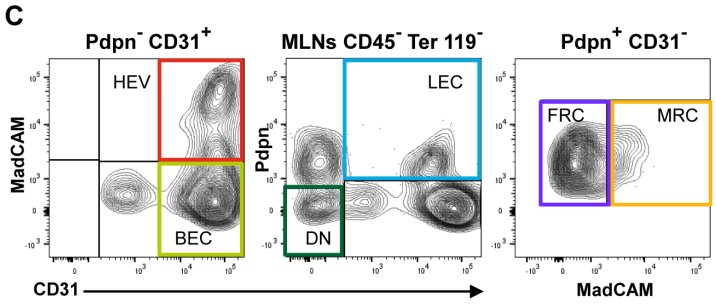

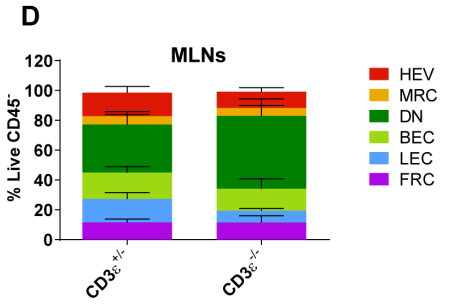

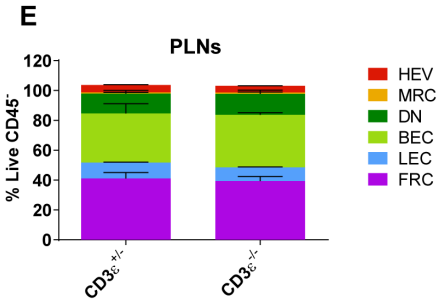

Legends to supplementary Figures:

Supplementary Figure 1 related to Figures 1 and 2: Regulation of ILCs by T cells and commensal bacteria in the Small Intestine Lamina Propria. (A) Flow cytometry analysis of ILCs from the Small Intestine Lamina Propria (SILP) of 8 weeks old T cell-deficient mice ($CD3\varepsilon^{-/-}$) and control littermates ($CD3\varepsilon^{+/-}$). Histograms showing the number of each ILC subset (**B**) and each ILC3 subset (**C**) in the SILP of T cell-deficient mice and control littermates before (3 weeks old $CD3\varepsilon^{-/-}$ n=7 and $CD3\varepsilon^{+/-}$ n=8) and after weaning (8 weeks old $CD3\varepsilon^{-/-}$ n=19 and $CD3\varepsilon^{+/-}$ n=14). (**D**) Flow cytometry analysis of IL-22 and IL-17A production by ILCs in the SILP of 8 weeks old T cell-deficient mice $CD3\varepsilon^{-/-}$ and control littermates $CD3\varepsilon^{+/-}$. (**E**) Histogram showing the number of ILCs expressing IL-22 alone or in combination with IL-17A in the SILP of 8 weeks old T cell-deficient mice $CD3\varepsilon^{-/-}$ (n=17) and control littermates $CD3\varepsilon^{+/-}$ (n=15). Histograms showing the percentage of each ILC (**F**) and each ILC3 subset (**G**) among $CD45^+$ cells in the SILP of 8 weeks old T cell-deficient mice and control littermate treated with a cocktail of broad-spectrum antibiotics ($CD3\varepsilon^{-/-}$ Abx n=9 and $CD3\varepsilon^{+/-}$ Abx n=7) or with glucose in the drinking water ($CD3\varepsilon^{-/-}$ SPF n=8 and $CD3\varepsilon^{+/-}$ SPF n=5). (**H**) Histogram showing the percentage of ILCs expressing IL-22 alone or in combination with IL-17A among $CD45^+$ cells in the SILP of 8 weeks old T cell-deficient mice and control littermate treated with a cocktail of broad-spectrum antibiotics ($CD3\varepsilon^{-/-}$ Abx n=9 and $CD3\varepsilon^{+/-}$ Abx n=7) or with glucose in the drinking water ($CD3\varepsilon^{-/-}$ SPF n=8 and $CD3\varepsilon^{+/-}$ SPF n=5). Histograms showing the number of each ILC (**I**) and each ILC3 (**J**) subset in the SILP of T cell-deficient mice injected with PBS (n=9), $CD4^+$ and $CD8^+$ T cells (n=6) or $CD4^+$ T cells (n=7), all mice were analyzed 12 weeks after the injection. (**K**) Histogram showing the number of ILCs expressing IL-22 alone or in combination with

IL-17A in the SILP of T cell-deficient mice in each experimental condition described above. Statistical analysis was performed using the 2 Way ANOVA method with alpha = 0.05. **** P<0.0001, *** P<0.001, ** P<0.01, * P<0.05. Data are pooled from at least 3 independent experiments. Data are represented as mean ± SEM.

Supplementary Figure 2 related to Figure 1: Cytokine production in each ILC subset. (**A** and **B**) Representative FACS plots showing the gating strategy used in order to discriminate each ILC subset based on the expression of RORγt, KLRG1 and NK1.1 in the MLNs (**A**) and SILP (**B**) of CD3ε$^{-/-}$ RORγt eGFP and CD3ε$^{+/-}$ RORγt eGFP littermates. (**C** and **D**) Flow cytometry analysis of cytokine production by each ILC subset in the MLNs (**C**) and SILP (**D**) of T cell-deficient mice and control littermates.

Supplementary Figure 3 related to Figure 3: T cell reconstitution and its effect on the composition of ILCs. (**A**) Histogram showing the percentage of donor derived cells in the MLNs and SILP 8, 12 and 16 weeks after the graft of thymic lobes from CD45.2 C57BL/6 neonates under the kidney capsule of CD45.1 CD3ε$^{-/-}$ recipients. (**B**) FACS dot plots showing the frequency of CD4^{+} and CD8^{+} T cells in the MLNs of T cell-deficient mice 16 weeks after thymus graft. MLNs from age-matched C57BL/6 are shown as controls. (**C**) Frequency of each ILC subset among recipient CD45^{+} Lin^{-} CD127^{+} cells in the MLNs 8 (n=6), 12 (n=6) and 16 (n=6) weeks after the graft. Representative flow cytometry analysis (**D**) and histogram (**F**) showing the percentage of donor cells among CD45^{+} cells in the MLNs, PLNs and SILP 12 weeks after the adoptive transfer of T cells as described in Figure 3. FACS dot plots (**E**) and histogram (**G**) showing the fraction of Ki67^{+} cell among donor derived cells in the same experimental conditions. (**H**) Representative flow cytometry analysis of the percentage

of Foxp3^{+} cells among donor derived CD4^{+} TCRβ^{+} cells in the MLNs and SILP. (**I**) Histogram showing the percentage of Foxp3^{+} cells among donor derived cells in the MLNs and SILP. Statistical analysis was performed using the 2 Way ANOVA method with CD3$\varepsilon^{-/-}$ mice as reference. Alpha = 0.05. **** P<0.0001, *** P<0.001, ** P<0.01, * P<0.05. Data are representative of 3 independent experiments. Data are represented as mean ± SEM.

Supplementary Figure 4 related to Figure 4: T cell deficiency does not impact the localization of ILC3s in mesenteric lymph nodes. Tissue sections from the MLNs of 8 weeks old CD3$\varepsilon^{+/-}$ (**A**) and CD3$\varepsilon^{-/-}$ (**B**) mice stained with anti-CD3 (Blue), anti-B220 (Red), anti-RORγt (Green). Pictures were taken using ZEISS ApoTome 2 Structured Illumination Microscope, objective 20x. Scale bar is 200 μm.

Supplementary Figure 5 related to Figure 4: T cell deficiency does not impact the composition of lymph node stromal cells. Tissue sections from the MLNs of 8 weeks old CD3$\varepsilon^{+/-}$ (**A**) and CD3$\varepsilon^{-/-}$ (**B**) mice stained with anti-Podoplanin (Pdpn) (blue), anti-MadCAM (red), anti-RORγt (green). MRC: Marginal Reticular cells. Pictures were taken using ZEISS ApoTome 2 Structured Illumination Microscope, objective 20x. Scale bar is 55 μm. (**C**) Gating strategy for the identification of lymph nodes stromal cell populations by flow cytometry. Histograms showing the frequency of stromal cell subsets among live CD45^{-} cells in the MLNs (**D**) and PLNs (**E**) of 8 weeks old CD3$\varepsilon^{+/-}$ (n=3) and

CD3$\varepsilon^{-/-}$ mice (n=3). High Endothelial Venules (HEV), Marginal Reticular Cells (MRC), DN (Double Negative), Blood Endothelial Cells (BEC), Lymphatic Endothelial Cells

(LEC), Fibroblastic Reticular Cells (FRC). Statistical analysis was performed using the 2 Way ANOVA method with alpha = 0.05. Data are represented as mean ± SEM.

Transparent Methods

Mice

CD45.1 CD3$\varepsilon^{-/-}$ mice (Malissen et al., 1995) were obtained from Benedita Rocha (INEM) and crossed with *Rorc(γt)-Gfp*^{TG} (Lochner et al., 2008) reporter mice in order to generate CD3$\varepsilon^{+/-}$ and CD3$\varepsilon^{-/-}$ *Rorc(γt)-Gfp*^{TG} littermates. CD45.1 CD3$\varepsilon^{-/-}$ mice were also maintained homozygous and used as recipients for T cell adoptive transfers. BAC-transgenic *Rorc(γt)-Gfp*^{TG} were provided by Gerard Eberl (Pasteur Institute). RAG2$^{-/-}$ OTII were provided by Nadine Cerf Bensussan (Imagine Institute) and Foxp3EGFP (Wang et al., 2008) mice by David Gross (INEM). IL-33$^{Gt/Gt}$ deficient mice were provided by Jean Philippe Girard (Pichery et al., 2012) (IPBS, Toulouse). All mice were maintained under specific pathogen free conditions (SPF). All experimental procedures using animals were approved by the "Comité d'éthique en experimentation animale" of the Paris Descartes University and the French Ministry of Research, Innovation and Education under the following reference APAFIS # 10246 N°201609161708233 v4.

Preparation of cell suspensions from small intestine lamina propria and lymph nodes

Mesentery and Peyer's patches were removed from the small intestine (Duodenum, jejunum and ileum) and its content was gently flushed out with ice cold PBS. The tissue was cut longitudinally and then transversally into 1 cm pieces and the epithelium was removed in PBS 30 mM EDTA for 30 min at 4°C. Tissue pieces were then vigorously shaken and washed in cold PBS 3 times. Tissue was further cut in smaller pieces and digested with 50 mg/mL collagenase D (Roche) and 10mg/mL DNase I (Sigma) in

DMEM, 2% FCS, 10 mM HEPES with continuous stirring at 37°C, 3 times for 15 minutes. After each incubation, tissue pieces were mechanically dissociated by repetitive pipetting through a 1 mL micropipette tip and the supernatant was filtered through a 70 µm cell strainer. Fresh digestion medium was added for the second and third digestions. Supernatants from successive digestions were pooled and suspended in 40% Percoll (GE Healthcare) layered on 80% Percoll. Hematopoietic cells were collected at the interface of the gradient and washed twice in DMEM, 10% FCS, 10 mM HEPES. Peripheral lymph nodes (inguinal, axillary, brachial, cervical) and mesenteric lymph nodes were teased with fine forceps and surrounding adipose tissue was removed. Lymph nodes were cut in small pieces and digested with 50 mg/mL collagenase D (Roche) and 10 mg/mL DNase I (Sigma) in DMEM, 2% FCS, 10 mM HEPES with continuous stirring at 37°C for 15 minutes. Tissue was then mechanically dissociated by repetitive pipetting through a 1 mL micropipette tip and the supernatant was filtered through a 70 µm cell strainer.

Ex vivo analysis of ILC composition and function

Multi-parametric flow cytometry analysis was performed on cell suspensions obtained from peripheral, mesenteric lymph nodes and small intestine lamina propria as described above. ILCs were identified as Lin^- $CD45^+$ $CD127^+$ cells among live lymphocytes with Lin including the following markers (CD3ε, TCRβ, TCRγδ, CD19, B220, CD11b, CD11c, Gr-1, Ter119). Among Lin^- $CD45^+$ $CD127^+$ cells, ILC1s were defined as $NKp46^+$ $ROR\gamma t^-$ $GATA3^-$ and ILC2s as $NKp46^-$ $ROR\gamma t^-$ $GATA3^{hi}$ (Fig. 1A). ILC3s were defined as $ROR\gamma t^+$ $GATA3^{lo}$ and further divided into $NKp46^+$, $CCR6^+$ and $NKp46^-$ $CCR6^-$ (DN) subsets (Fig. 1D). Transcription factors were detected using the Foxp3 detection kit from eBiosciences. Cytokine production (IL-5, IL-13, IL-17A and

IL-22) was assessed after *ex-vivo* re-stimulation in complete culture medium for 3h in the presence of 100 ng/ml of phorbol 12-myristate 13-acetate (PMA), 1 µg/ml of Ionomycin and 10 µg/ml of Brefeldine A. When IL-22 secretion was assessed, re-stimulation was performed in the presence of 40 ng/mL rmIL-23 (Immuno Tools). For intra-cellular cytokine staining, cells were stained first for cell surface markers and then fixed with PBS Paraformaldehyde 2% washed and permeabilized in MACS buffer 0,5% Saponin. Flow cytometry data were acquired using FACS Canto II and LSR Fortessa SORP (Becton Dickinson) and analyzed using the FlowJo software (Tristar).

Antibodies for flow cytometry analysis

Live/Dead Fixable Aqua staining (Invitrogen) was used for live/dead cell discrimination. Antibodies specific for lineage markers were purchased from eBioscience and Sony Biotechnology. FITC, PE or Biotin-conjugated antibodies were used for the detection of lineage markers: CD3ε (145-2C11), TCRβ (H57-597), TRCγδ (GL3), CD19 (6D5), B220 (RA3-6B2), CD11b (M1/70), CD11c (HL3), Gr-1 (RB6-8C5), Ter-119 (TER-119). The following antibodies were used for the detection and the identification of ILCs: APC-eF780 anti CD45.1 (A20), PerCP-Cy5.5 anti CD45.2 (104), PE-Cy7 anti CD127 (A7R34), Biotin anti NKp46 (29A1.4), BV605 anti CCR6 (29-2L17), BV786 anti Ki67 (B56), APC anti RORγt (AFKJS-9), PE anti GATA-3 (TWAJ), APC anti IL-5 (TRFK5), PE anti IL-13 (ebio13A), APC anti IL-17A (ebio17B7), PE anti IL-22 (1H8PWSR).

Antibiotics treatment from birth

Pregnant mice were isolated around two weeks post coitum and treated with a cocktail of broad-spectrum antibiotics (Ampicillin 0,5g/L; Streptomycin 1g/L; Metronidazol 0,5g/L in 2% Glucose) in the drinking water. After birth, mothers and pups were treated

with the same cocktail of antibiotics in their drinking water. Pups were weaned around four weeks of age and treated until euthanized for tissue collection at 8 weeks of age. When grafted with T cells, recipients remained under antibiotic treatment until euthanized for tissue collection and flow cytometry analysis.

Thymic lobe graft

Thymic lobes were isolated from C57BL/6J or *Rorc(γt)-Gfp*^{TG} neonates and grafted under the kidney capsule of 8 weeks old CD45.1 CD3$\varepsilon^{-/-}$ recipient mice as previously described (Berzins et al., 1998). Briefly, thymic lobes were collected from neonates and kept on sterile ice cold DMEM until the graft was performed. Recipient mice were anesthetized with a cocktail of Ketamin (10 mg/mL) and Xylazin (1,2 mg/mL) and one kidney was exposed and gently plucked to perform a 2-3 mm incision into which one thymic lobe was inserted. Wounds were then surgically stitched and washed with Vétédine®. Control recipients were injected with PBS. Mice were sacrificed for tissue collection and multi-parametric flow cytometry analysis 8, 12 and 16 weeks later.

Adoptive transfers of T cells

Donor T cells were isolated from the peripheral lymph nodes and spleen of C57BL/6J mice and sorted using a FACSAria III (Becton Dickinson). Bulk CD4$^+$ and CD8$^+$ T cells were separated and a combination of 1,5.10^6 cells of each CD4$^+$ and CD8$^+$ T cells or 3.10^6 CD4$^+$ T cells were injected intravenously into CD45.1 CD3$\varepsilon^{-/-}$ mice. Foxp3$^+$ CD4$^+$ T cells were isolated from Foxp3EGFP mice (Wang et al., 2008) and 1.10^6 cells were injected into CD45.1 CD3$\varepsilon^{-/-}$ mice. CD4$^+$ T cells were isolated from the spleen and lymph nodes of RAG2$^{-/-}$ OTII TCR transgenic mice and 3.10^6 cells were injected intravenously into CD45.1 CD3$\varepsilon^{-/-}$ mice. When specified, Ovalbumin (1,5%) and

Glucose (0,5%) were given in the drinking water of recipient mice for the whole duration of the procedure. Control recipients were injected with PBS. Adoptively transferred mice and control mice injected with PBS were sacrificed for tissue collection and multi-parametric flow cytometry analysis 12 weeks later.

RT-qPCR analysis

Freshly collected mesenteric lymph nodes, peripheral lymph nodes, and distal ileum from 8 weeks old CD3$\varepsilon^{-/-}$ and CD3$\varepsilon^{+/-}$ mice were incubated in RNAlater for 12h at 4°C (Ambion) and then frozen at -80°C. Total RNAs were extracted using the RNeasy mini Kit from Qiagen. cDNA was synthetized using the MuLV Reverse transcriptase (Thermofisher) according to the manufacturer's instructions. For qPCR analysis, specific primers for il33, il25, Tslp, and Hprt were purchased from Qiagen. Gene detection and gene quantification were performed using the SYBRGreen master mix from Qiagen and the ABI 7900HT real-time PCR system. Lymph node stromal cells (CD45^{-}) were sorted from the mesenteric lymph nodes after enzymatic digestion and depletion of CD45^{+} cells. Total RNA was extracted using the RNeasy micro Kit from Qiagen. Linear amplification of total RNA was performed using the message Booster kit (Ambion). cDNA was synthesized using SuperScript Reverse Transcriptase (Invitrogen) and qPCR analysis was performed as described above.

Treatment with neutralizing antibodies

Age-matched CD3$\varepsilon^{-/-}$ mice were injected once intra-peritoneally with purified blocking antibody or istotype control and sacrificed 24 hours later for tissue collection and flow cytometry analysis. The amounts of antibody or isotype control that were injected are 200 μg of anti-ST2/IL-33R (clone 245707, R&D systems) or Rat IgG2b, 500 μg of anti-

IL-17RB (clone D9.2 kindly provided by Andrew Mac Kenzie) or Rat IgG1 and 20 μg of anti TSLP (clone 152614, R&D systems) or Rat IgG2a.

Bone marrow chimera

8 weeks old C57BL/6 or IL-33$^{Gt/Gt}$ deficient mice were lethally irradiated and reconstituted with 2.10^{6} of lineage depleted bone marrow cells from CD45.1 CD3$\varepsilon^{-/-}$ mice. Mice were sacrificed for tissue collection and multi-parametric flow cytometry analysis 8 weeks later.

Statistical analysis

Statistical analysis was performed using the Prism software (GraphPad) and statistical significance was determined using Two-way Anova or unpaired Mann Whitney statistical tests as indicated in the figure legends.

Supplemental References:

Berzins, S.P., Boyd, R.L., and Miller, J.F.A.P. (1998). The Role of the Thymus and Recent Thymic Migrants in the Maintenance of the Adult Peripheral Lymphocyte Pool. J Exp Med *187*, 1839-1848.

Lochner, M., Peduto, L., Cherrier, M., Sawa, S., Langa, F., Varona, R., Riethmacher, D., Si-Tahar, M., Di Santo, J.P., and Eberl, G. (2008). In vivo equilibrium of proinflammatory IL-17+ and regulatory IL-10+ Foxp3+ RORgamma t+ T cells. J. Exp. Med. *205*, 1381–1393.

Malissen, M., Gillet, A., Ardouin, L., Bouvier, G., Trucy, J., Ferrier, P., Vivier, E., and Malissen, B. (1995). Altered T cell development in mice with a targeted mutation of the CD3-epsilon gene. EMBO J *14*, 4641–4653.

Pichery, M., Mirey, E., Mercier, P., Lefrancais, E., Dujardin, A., Ortega, N., and Girard, J.-P. (2012). Endogenous IL-33 Is Highly Expressed in Mouse Epithelial Barrier Tissues, Lymphoid Organs, Brain, Embryos, and Inflamed Tissues: In Situ Analysis Using a Novel Il-33–LacZ Gene Trap Reporter Strain. J. Immunol. *188*, 3488-3495.

Wang, Y., Kissenpfennig, A., Mingueneau, M., Richelme, S., Perrin, P., Chevrier, S., Genton, C., Lucas, B., DiSanto, J.P., Acha-Orbea, H., et al. (2008). Th2 Lymphoproliferative Disorder of Lat^{Y136F} Mutant Mice Unfolds Independently of TCR-MHC Engagement and Is Insensitive to the Action of Foxp3^{+} Regulatory T Cells. J. Immunol. *180*, 1565-1575.